

September 1995



-Instituut voor Plasmafysica Rijnhuizen • Associatie Euratom-FOM

Postbus 1207
3430 BE Nieuwegein
Nederland
Edisonbaan 14
3439 MN Nieuwegein
Tel. 30-6096999
Fax. 30-6031204

ELIXER, a simulation code for the spatial structure of light pulses in Free-Electron Lasers

G.H.C. van Werkhoven

The author likes to thank prof.dr. T.J. Schep, dr. B. Faatz for discussions regarding the development of the FEL model, and prof.dr. J.P. Goedbloed and dr.S. Poedts for the availability of the REVISE package.

This work was performed as part of the research programme of the Stichting voor Fundamenteel Onderzoek der Materie (FOM) with financial support from the Nederlandse Organisatie voor Wetenschappelijk Onderzoek (NWO).

RIJNHUIZEN
REPORT
95-226



Abstract

This report discusses the simulation code ELIXER, which was developed to study the spatial evolution of radiation in pulsed-beam Free-Electron Lasers. ELIXER includes the full spatial structure of the radiation by means of a set of orthogonal axisymmetric Gauss-Laguerre functions. Reflection and transmission on realistic cavity mirrors is included by means of a matrix formulation. The code differs from other spatially three dimensional models by calculating the longitudinal electron dynamics for each electron separately, whereas the transverse motions are approximated by the variation of the radial beam envelope. This approximation leads to a significant reduction of the numerical effort.

An overview of the physical model is presented, and the numerical implementation of the FEL equations in the code is discussed. Particular emphasis is put on the input file, which describes the FEL device that is to be simulated, and on the output files that contain the spatial and spectral properties of the radiation, as well as the energy spectrum of the beam electrons.

Contents

1	Free-Electron Laser Model	3
1.1	Introduction	3
1.2	Density-averaged FEL equations	5
1.2.1	Electron Dynamics	5
1.2.2	Radiation Dynamics	7
1.2.3	Segment division and mode of beam operation	8
1.3	Application to a hole-coupled axisymmetric resonator	9
1.3.1	Gauss-Laguerre basisfunctions	10
1.3.2	Power and spectral power distributions over the transverse modes	11
1.3.3	Reflection and transmission	13
1.3.4	Optical beam clipping by the vacuum tube	15
1.4	Initial conditions for the electron and radiation pulses	15
2	Numerical Implementation	17
2.1	ELIXER working equations	17
2.2	Numerical control parameters and integration method	19
2.3	Grids points and array dimensions	21
3	Working with ELIXER	25
3.1	Getting started	25
3.2	Input file	26
3.2.1	Numerical control parameters	26
3.2.2	Undulator parameters	27
3.2.3	Cavity parameters	27
3.2.4	Electron initial conditions	28
3.2.5	Radiation initial conditions	30
3.2.6	Miscellaneous parameters	30
3.3	Output files	31
3.3.1	Matrix elements : matrix.data	31
3.3.2	Optical mode structure in the undulator : optic1.data and optic1av.data	33
3.3.3	Optical mode structure at the downstream mirror : optic2.data and optic2av.data	35

3.3.4	Optical mode structure at the upstream mirror : optic3.data and optic3av.data	37
3.3.5	Optical power spectrum : ospec1.data (inside the undulator), ospec2.data (at the downstream mirror), ospec3.data (at the upstream mirror)	39
3.3.6	Electron orbits : orbit.data	40
3.3.7	Electron energy spectrum : espec.data	41
A	Pre-compilation using the REVISE package	43
A.1	Installation of REVISE	44
B	Calculation of the radiation amplitude using RADPROF	47

Chapter 1

Free-Electron Laser Model

1.1 Introduction

Simulation codes for the self-consistent computation of the electron and wave dynamics in Free Electron Lasers (FELs) are important tools for understanding of FEL physics in realistic geometries, as well as for the design of new FEL experiments. The most basic simulation code, which has been developed by Colson [1], describes the longitudinal dynamics of the radiation and electron beams, and the induced transverse velocity. The model depends on only one spatial coordinate (the position along the undulator z) and is therefore generally referred to as the 1D model. The model describes most basic features of FEL operation, as gain and saturation, sideband modes and finite pulse effects, and can be used for basic understanding or to make rough estimates of FEL parameters.

The 1D approximation has only a limited validity for a quantitative comparison with FEL experiments, for two reasons. In the first place, a more realistic description of the transverse motions of the electron is required for realistic beam sizes. When the beam is injected into the undulator, ‘warm’ beam effects as emittance cause the beam to diverge. The focussing property of the undulator magnet compensate for this effect, but leads to a slow periodic modulations of the beam, the betatron oscillation. In the second place, the electron beam tends to focus the optical beam towards the electrons. This implies that the radial profile of the light will change due to the interaction. Also diffraction of the radiation on the cavity mirrors leads to a time-dependent radial profile. In a hole coupled resonator, the radial structure of the intra-cavity radiation will change from pass to pass. In such a cavity geometry, the radial profile is determined by the competing mechanisms of power loss through the aperture, which tends to reduce the on-axis field intensity, and by the gain due to the interaction with the electrons, which tends to restore the radial profile.

The influence of these three dimensional (3D) effects have sofar been investigated for long and uniform electron beams, thereby neglecting finite pulse effects [2]. The latter assumption is valid as long as the pulse length is larger then the slippage length $L_{slip} = N_{und}\lambda$, which is the distance between the light and electron pulses that is induced by the velocity difference between the pulses. However, the length of electron pulses that are accelerated by an rf-linac (which is used most existing FELs) can be a fraction of

the slippage length. For instance, the pulse length in both FELs of the Dutch FEL user facility FELIX [3] can be down to one tenth of the slippage length. This implies that the radiation pulse overtakes the electron pulse while traversing the undulator, and thus, interacts with the electrons for a fraction of the transit time. This affects the balance between gain and aperture loss and has important consequences for the spatial structure of the generated optical pulses [4, 5]. However, 3D simulation codes that include finite pulse effects are hardly tractable from the computationally point of view, although a few of them exist [6, 7]. The required computing time is typically several hours of Cray-time.

For this reason an approximate simulation code has been developed, ELIXER, that limits the computational effort to acceptable proportions. The code includes short pulse effects and accounts for a number of 3D effects. The main assumption is that the transverse electron dynamics are modelled by the radial envelope of the electron beam, rather than by the transverse motion of each electron separately. Emittance and betatron oscillations are included through a variation of the beam envelope. The radial inhomogeneity of the radiation field, which yields a different ponderomotive force for on-axis and off-axis electrons, is accounted for by averaging the longitudinal motion over the radial density profile of the beam. This procedure, in combination with the beam envelope formulation, reduces the electron dynamics to effectively one dimensional motions. The spatial structure of the paraxial radiation is accounted for by means of a finite number of radially orthogonal basisfunctions. Although this approach allows to simulate a-symmetric cavities and waveguides, ELIXER employs axisymmetric Gauss-Laguerre basisfunctions. This restricts the applicability of the code to an axisymmetric FEL resonator FEL, which consists of two circular, spherically curved mirrors that are perfectly aligned. The intra-cavity radiation can be coupled out through a on-axis hole in either one of the mirrors. The code was tested against a spatially one dimensional model in case the radial profile is dominated by a single transverse mode, and against the simulation code TDA, which assumes a continuous electron beam. For FEL parameters close to those of FELIX, ELIXER was found in excellent agreement with TDA [8]. Recently, the code has been used to interpretate experimental results regarding the transverse structure of the radiation in the FEL resonators of FELIX [9, 10, 11].

This report is organized as follows. In this Chapter the FEL model is presented. An overview of the density-averaged set of electron-wave equations is presented in Section 1.2, and in Section 1.3 the model is applied to an axisymmetric FEL resonator. Section 1.4 discusses the initial conditions of the electron and radiation pulses. Aspects of the numerical implementation of the FEL model in the ELIXER code, which is written in FORTRAN 77, are presented in Chapter 2. Particular emphasis is put on integration schemes and numerical control parameters. Chapter 3 discusses how the code can be obtained, its (pre-)compilation using the REVISE package, the FEL parameters in the input file, and the output files that contain the spatial and spectral structure of the radiation pulse, and the energy spectrum of the beam electrons.

1.2 Density-averaged FEL equations

In this Section an overview of the FEL model that is implemented in ELIXER is given since the model has been discussed extensively elsewhere [4, 12]. An FEL is considered with a static undulator, with N_u periods of size λ_u . The undulator has either helical or planar geometry. The helical polarized magnetic field in a helical undulator is represented by the vector potential

$$\mathbf{A}_u(\mathbf{x}, z) = -A_u(\mathbf{x})[\mathbf{e}_x \cos(k_u z) + \mathbf{e}_y \sin(k_u z)], \quad (1.1)$$

and the linear polarized magnetic field (in the y -direction) of the planar undulator is

$$\mathbf{A}_u(\mathbf{x}, z) = -\sqrt{2}A_u(\mathbf{x})\mathbf{e}_y \sin(k_u z), \quad (1.2)$$

where the undulator strength $A_u = |\mathbf{A}_u|$ is given by

$$A_u(\mathbf{x}) = A_{u0}(1 + k_x^2 x^2 + k_y^2 y^2). \quad (1.3)$$

All potentials are normalized to units of e/mc . The values of k_x and k_y depend on the undulator geometry, i.e. $k_x = k_y = k_u/\sqrt{2}$ in a helical undulator and $k_x = k_u$, $k_y = 0$ in a planar geometry. The radiation field is assumed to be dominated by a single longitudinal mode with frequency $\omega = ck$

$$\mathbf{A} = ue^{+ik(z-ct)}\mathbf{e}_+ + u^*e^{-ik(z-ct)}\mathbf{e}_- \quad (1.4)$$

where u is slowly varying complex amplitude, and $\mathbf{e}_\pm = (\mathbf{e}_x \pm i\mathbf{e}_y)/2$ are circularly polarized vectors. The radial dependence of u is described by a set of transverse basisfunctions

$$u = \sum_{n,m} u_{nm} \Psi_{nm}, \quad (1.5)$$

that satisfy the paraxial wave equation in vacuum

$$(\partial_x^2 + \partial_y^2 + 2ik\partial_z)\Psi_{nm} = 0. \quad (1.6)$$

The latter result can be obtained from Maxwell's equations under the assumption that the radiation propagates within an angle of 30° from the longitudinal axis.

1.2.1 Electron Dynamics

Starting point for the description of the model are the electron equations of motion. The longitudinal electron dynamics is determined by the *ponderomotive* potential, which arises due to the coupling between electro-magnetic field and the induced transverse current. The longitudinal motion is described by the ponderomotive phase

$$\psi = (k + k_u)z - \omega t = (k + k_u)(z - v_{pont}t), \quad (1.7)$$

where $v_{pont} = \omega/(k + k_u)$ is the phase velocity of the ponderomotive wave, and by the energy

$$\delta\gamma = \gamma - \gamma_r, \quad (1.8)$$

where γ_r is the resonant energy. The latter is defined as the energy where the longitudinal electron velocity $v_z \simeq c(1 - \mu_e^2/2\gamma_r^2)$ is equal to v_{pon} . This resonance condition implies that

$$\omega = ck_u 2\gamma_r^2 / \mu_e^2, \quad (1.9)$$

where the effective mass μ_e^2 consists of the ‘cold’ contribution $1 + A_{u0}^2$, and of a ‘warm’ part that arises due to the transverse motions (x, P_x) , (y, P_y) of the beam electrons. ELIXER differs from other 3D models by including the full longitudinal electron motion, whereas the transverse electron motion is only approximately accounted for. The main assumption is that the transverse motion of the electron beam can be described by a Gaussian radial density profile

$$n \propto \frac{1}{2\pi\sigma_x\sigma_y} e[-(x^2/2\sigma_x^2 + y^2/2\sigma_y^2)], \quad (1.10)$$

where $\sigma_x(z, z - v_{pon}t) = \sqrt{\langle x^2 \rangle}$ is the beam envelope in the x -direction. The brackets $\langle \dots \rangle$ denote a density average over the transverse dimensions of the beam, and the time-coordinate $z - v_{pon}t$ is used to emphasize the pulse character of the electron beam, which velocity must be close to v_{pon} for FEL interaction to occur. The z -dependence of the beam envelopes σ_x and σ_y is governed by the natural divergence of the beam electrons, due to a finite emittance, and by the focusing properties of the undulator field, which will give rise to a slow ‘betatron’ oscillation of the electron orbits. The evolution of σ_x is given by the following expression [4]

$$\sigma_x(z, z - v_{pon}t) = \sigma_{x0}(z - v_{pon}t)[1 + (r_{\beta x}^2 - 1) \sin^2 \kappa_{\beta x} z]^{\frac{1}{2}}, \quad (1.11)$$

where $\sigma_{x0}(z - v_{pon}t)$ is the typical spotsize of the beam at the entrance of the undulator, $\kappa_{\beta x} = A_{u0}k_x/\gamma_r$ is the betatron wavenumber and $r_{\beta x} = (\epsilon_x/4\pi A_{u0}k_x\sigma_{x0}^2)$ determines the amplitude of the oscillation. Here ϵ_x is the normalized emittance of the electron pulse¹

$$\epsilon_x(z - v_{pon}t) = 4\pi[\langle x^2 \rangle \langle P_x^2 \rangle - \langle x P_x \rangle^2]^{1/2}, \quad (1.12)$$

P_x being the electron’s generalized transverse momentum (normalized to mc). Equation (1.11) is obtained by neglecting the small variation in energy in the equations of transverse motion, such that they can be solved independently of the longitudinal motion, and by averaging the resulting equations over an undulator period. A similar equation describes the evolution of the envelope σ_y in the y -direction. The betatron parameters κ_β and r_β are explicitly written down for the different undulator geometries. In the case of a helical undulator, an electron beam is considered with equal radii and emittance in both directions, $\sigma_{x0} = \sigma_{y0}$ and $\epsilon = \epsilon_x = \epsilon_y$. This leads to ($\kappa_\beta = \kappa_{\beta x} = \kappa_{\beta y}$ and $r_\beta = r_{\beta x} = r_{\beta y}$)

$$\kappa_{beta} = \frac{A_{u0}k_u}{\sqrt{2}\gamma_r}, \quad r_\beta = \frac{\epsilon}{4\pi\gamma_r \kappa_\beta \sigma_{x0}^2}. \quad (1.13)$$

¹The normalized emittance is a constant of transverse motion in the case of an undulator with a linear focussing force, i.e. Eq. (1.3).

For the planar undulator, the result is ($\kappa_{\beta y} = r_{\beta y} = 0$)

$$\kappa_{\beta x} = A_{u0}k_u/\gamma_r, \quad r_{\beta x} = \frac{\epsilon_x}{4\pi\gamma_r \kappa_{\beta x}\sigma_{x0}^2}. \quad (1.14)$$

The expressions for the beam envelopes are used to define the effective mass μ_e^2 , which enters the FEL-relation Eq. (1.9). In a ‘warm’ beam, the effective mass is in principle different for each electron, since each electron has its own ‘temperature’ [12]. Thus, each electron has its own resonant condition. This phenomenon is partially accounted for in the FEL relation Eq. (1.9) by including the effective mass, averaged over the cross-section of the beam

$$\mu_e^2 = 1 + A_{u0}^2[1 + k_u^2\sigma_{x0}^2(1 + r_\beta^2)]. \quad (1.15)$$

This expression is valid for a helical undulator, but can also be used in a planar undulator, upon replacing r_β by $r_{\beta x}$.

The longitudinal $(\psi, \delta\gamma)$ electron dynamics is coupled to the transverse motions mainly through the radial inhomogeneity of the undulator and radiation fields. This causes on-axis electrons to experience a different ponderomotive force as compared to off-axis electrons. This effect is approximately accounted for by averaging the equations of longitudinal motion over the radial density of the beam. Since the transverse profile of the radiation is determined by the basisfunctions Ψ_{nm} , the density-average can be calculated analytically. The resulting averaged equations of motion are

$$\frac{d\psi}{dz} = 2k_u \frac{\delta\gamma}{\gamma_r}, \quad (1.16)$$

$$\frac{d\delta\gamma}{dz} = i \frac{kA_{u0}}{2\gamma_r} \sum_{n,m} (I_{nm}u_{nm}e^{i\psi} - I_{nm}^*u_{nm}^*e^{-i\psi}), \quad (1.17)$$

where the radiation amplitudes u_{nm} has to be evaluated at the electron’s pulse position $z - v_{pont}t = \psi/(k + k_u)$, and the complex function

$$I_{nm}(z, z - v_{pont}t) = \int d^2\mathbf{x} \frac{1}{2\pi\sigma_x\sigma_y} e^{[-(x^2/2\sigma_x^2 + y^2/2\sigma_y^2)]} \Psi_{nm}(\mathbf{x}, z) \quad (1.18)$$

denotes the density average. The terms $(k_x^2x^2 + k_y^2y^2)$, which arise from the radial inhomogeneity of the undulator, have been neglected in Eq. (1.18). Note that I_{nm} includes the beam envelopes σ_x and σ_y , which vary along the undulator according to Eq. (1.11).

1.2.2 Radiation Dynamics

Using the decomposition Eq. (1.5), the following set of coupled wave equations for the radiation coefficient u_{nm} can be obtained [4]

$$\partial_z u_{nm}(z, z - ct) = i(2\pi\sigma_{x0}\sigma_{y0})f_B^2 \frac{\omega_p^2}{c^2} \frac{A_{u0}}{2k} \frac{I_{nm}^*}{w_{nm}^2} \mathcal{X} \frac{1}{N} \sum_{j=1}^N e^{-i\psi_j}(z, z - v_{pont}t). \quad (1.19)$$

where the radiation coefficient u_{nm} is considered to be a function of time coordinate $z - ct$ instead of $z - v_{pon}t$. This has the advantage that both the wave equation can be written as an ordinary differential equation. The relation between the time-coordinates,

$$z - ct = \frac{c}{v_{pon}} \left[(z - v_{pon}t) - \left(1 - \frac{v_{pon}}{c}\right)z \right] \quad (1.20)$$

expresses the slippage between the electron and radiation pulses. The source term (right hand side of Eq. (1.19)) consists of the product of the beam density, which has been approximated by the Gaussian profile Eq. (1.10), and the basisfunction Ψ_{nm} , averaged over the transverse dimensions. This average, which is similar to the density averaging procedure that was applied to the electron equations of motion, can be denoted by the complex conjugate of the density average I_{nm} , divided by the spotsize $w_{nm}^2 = \int d\mathbf{x} |\Psi_{nm}|^2$ of each transverse mode. The spatial bunching of electrons, which is measured by the bunching factor $\exp(-i\psi_j)$ of each electron j , is the driving force for coherent amplification of the radiation. The radiation and the source term are averaged over a distance Δ in the coordinate $z - v_{pon}t$, thereby keeping the position z fixed. This implies that, at position z , the source term consists of the contribution $e^{-i\psi_j}$ of all $N(z, z - v_{pon}t)$ electrons that are located within the interval

$$z - v_{pon}t \leq \psi_j(z)/(k + k_u) < z - v_{pon}t + \Delta. \quad (1.21)$$

The longitudinal density profile of the electron pulse is represented by the dimensionless function

$$\mathcal{X}(z, z - v_{pon}t) = \frac{1}{n_0} \frac{N}{2\pi\sigma_{x0}\sigma_{y0}\Delta}, \quad (1.22)$$

where $2\pi\sigma_{x0}\sigma_{y0}$ is the radial cross-section of the beam at the entrance of the undulator, and $n_0 = I/(ec2\pi\sigma_{x0}\sigma_{y0})$ is the peak beam density, I being the peak current. The segment size Δ depends on the longitudinal homogeneity of the electron pulse. This will be discussed in Section 1.2.3. Furthermore, $\omega_p^2 = e^2n_0/\epsilon_0m\gamma_r$ is the relativistic plasma frequency, and the parameter f_B arises from averaging the electron and wave equations over an undulator period².

1.2.3 Segment division and mode of beam operation

Due to its slowly varying character of the radiation, the optical pulse can be thought of as being divided into segments of constant u_{nm} with size of an optical wavelength $\lambda = 2\pi/k$ in the $z - ct$ -coordinate. This segment size corresponds to segments $\Delta = \lambda_{pon} = 2\pi/(k + k_u)$ of a *ponderomotive* wavelength in the electron coordinate $z - v_{pon}t$. Whether this segment division can also be applied to the electron pulse depends on the level of non-uniformity Λ of the longitudinal beam density, where

$$\Lambda = (k + k_u)^{-1} \partial_{(z-v_{pon}t)} \ln(n). \quad (1.23)$$

²This parameter is equal to unity for a helical undulator ($f_B = 1$), and is given by $f_B = J_0(\Delta) - J_1(\Delta)$ in a planar undulator type, Δ being equal to $A_{u0}^2/2(1 + A_{u0}^2)$.

It can be shown that the number of electrons N per segment is constant for all values of the energy detuning of practical interest, if the electron pulse is nearly constant over a ponderomotive wavelength ($\Lambda \ll 1$) [12]. This implies that, besides the radiation pulse, also the electron pulse can be divided into segments with size $\Delta = \lambda_{pon}$, over which the beam density \mathcal{X} is constant. This *constant density approximation* allows to compute the source term at each segment, which is also a ponderomotive bucket since ψ increases with 2π over the segment, from the number N of electrons that were initially in the bucket. All electrons in the bucket are assumed to experience the same radiation amplitude.

A special case of $\Lambda \ll 1$ is a continuous electron beam, in which the electron pulses are long and uniform such that $\Lambda = 0$. The generated light pulses will have the same pulse profiles. This implies that the slippage between the pulses is a subdominant process, such that the difference between the time coordinates $z - ct$ and $z - v_{pon}t$ can be neglected. Only the electron-wave dynamics in a *single* ponderomotive bucket has to be considered, since the electrons experience the same radiation field throughout the pulse.

The division of the electron pulse into λ_{pon} -segments can not be used if the beam density profile changes considerably over a ponderomotive wavelength ($\Lambda = \mathcal{O}(1)$), as for pulses that are several wavelengths long. In that case the electron and radiation pulses have to be divided into *smaller* segments, $\Delta < \lambda_{pon}$. Although the radiation amplitude is constant over this time interval, this is certainly not the case for the beam density since the electrons migrate to neighbouring segments due to a non-zero energy detuning or due to the electron synchrotron motion. Therefore a particle tracking method is used, in which the source term in a particular segment $z - v_{pon}t$ is constructed by tracking down all electrons that are presently located in that segment, and in which the electrons experience the radiation field at their present position in the pulse, given by $\psi_j/(k + k_u)$.

Summarizing the discussion above, three different modes of (electron beam) operation can be distinguished :

- *Pulsed beam operation with particle tracking* ($\Lambda = \mathcal{O}(1)$),
- *Pulsed beam operation with constant density approximation* ($\Lambda \ll 1$),
- *Continuous beam operation with constant density approximation* ($\Lambda = 0$).

The segment size for the latter two modes of operation is $\Delta = \lambda_{pon}$, whereas smaller segments are allowed in the first case.

1.3 Application to a hole-coupled axisymmetric resonator

The model is applied to an FEL in an axisymmetric resonator configuration. The resonator consists of two circular, spherically curved mirrors, which are perfectly aligned.

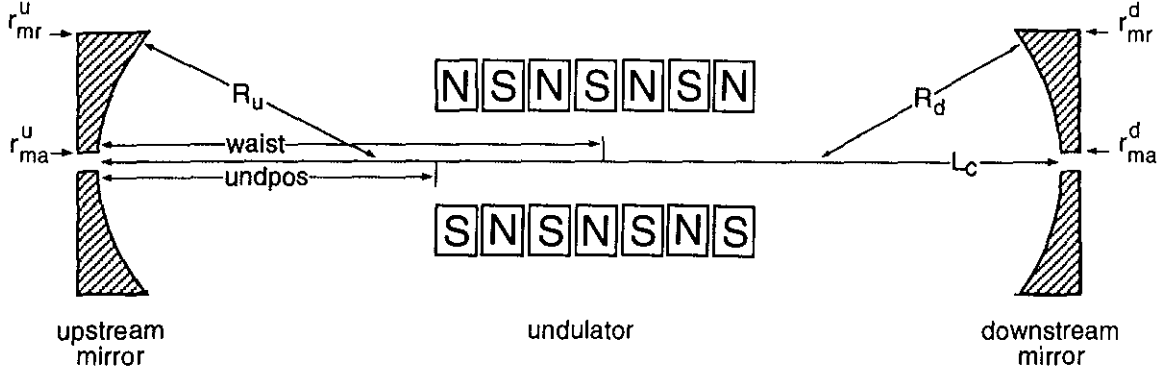


Figure 1.1: Schematic layout of the resonator.

The hole is in either one of the mirrors, as is shown in Fig. 1.1. An axisymmetric radiation field $u(r, z)$ can be considered, in the case that the interaction with the electron beam does not give rise to asymmetries. This requires in principle an FEL with a helical undulator, electron pulses with equal emittance in both transverse directions, and an axisymmetric Gaussian density profile. However, also a planar undulator can be considered, as long as betatron oscillations remain at a low level.

1.3.1 Gauss-Laguerre basisfunctions

ELIXER describes the radial dependence of the radiation in terms of a finite number of Gauss-Laguerre (GL) basisfunctions³ Ψ_n with z -dependent coefficients (the index m is neglected because of axisymmetry)

$$u(r, z, z - ct) = \sum_{n=0}^M u_n(z, z - ct) \Psi_n(r, z), \quad (1.24)$$

$$\Psi_n = \frac{s_0}{s} e^{-i\zeta_n - (1-i\alpha)\xi/2} L_n(\xi), \quad (1.25)$$

where $L_n(\xi)$ is the n -th Laguerre polynomial with argument $\xi = 2r^2/s^2$, $s^2 = s_0^2(1+\alpha^2)$, $s_0^2 = 2l_r/k$ is the minimum spotsize of the field, $\alpha = (z - z_w)/l_r$ and $\zeta_n = (2n + 1)\arctan \alpha$. Note that since $L_0 = 1$, the lowest GL function ($n = 0$) has a Gaussian radial profile. The Rayleigh length l_r and waist position z_w can be chosen such that the optical phase front exactly matches the radii of curvatures R_u and R_d of the 'upstream' ($z = 0$) and 'downstream' ($z = L_c$) mirrors

$$z_w = \frac{(R_d - L_c)L_c}{R_u + R_d - 2L_c}, \quad l_r = \sqrt{z_w(R_u - z_w)}, \quad (1.26)$$

L_c being the cavity length. The radial intensity profile of each GL function is shown in Fig. 1.2. Note that the radial extension of the GL functions increases with the mode number n .

³The GL functions are solutions of the wave equation $(r^{-1}\partial_r r \partial_r + rik\partial_z)\Psi_n = 0$.

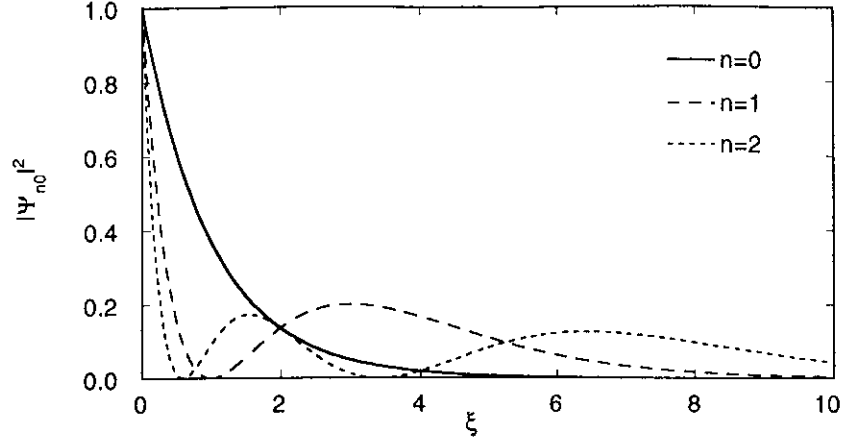


Figure 1.2: The power distribution $|\Psi_n|^2$ as a function of the radial coordinate ξ . Only the lowest GL functions are shown ($n = 0, 1$ and 2).

The density averaged I_{nm} and the spotsize w_{nm}^2 , which enters the set of averaged equations, can now be calculated since the basisfunctions are explicitly known. The result is (neglecting the index m)

$$I_n(z, z - v_{pon}t) = \frac{1}{1 + i\alpha + \sigma_b} \left(\frac{1 - i\alpha - \sigma_b}{1 + i\alpha + \sigma_b} \right)^n, \quad (1.27)$$

$$w_n^2 = w^2 = \pi s_0^2 / 2, \quad (1.28)$$

where $\sigma_b = 4\sigma_x^2(z, z - v_{pon}t) / s_0^2$. Nota that the spotsize is independent of the mode number.

1.3.2 Power and spectral power distributions over the transverse modes

The expansion of the radiation into GL functions can be employed to obtain the distribution of the radiation power and the spectral power over the transverse modes. The radiation power, P_{tot} , is the energy density of the electro-magnetic field that flows with speed c through a plane perpendicular to the (z) -direction of propagation

$$P_{tot}(z, z - ct) = 2\pi \int_0^\infty r dr \frac{1}{2} (\epsilon_0 |\mathbf{E}|^2 + \mu_0^{-1} |\mathbf{B}|^2) c. \quad (1.29)$$

Upon inserting the electric and magnetic fields \mathbf{E} and \mathbf{B}

$$\mathbf{E} = -\partial_t \mathbf{A} \simeq ick \sum_{n=0}^M [u_n \Psi_n e^{+ik(z-ct)} \mathbf{e}_+ - u_n^* \Psi_n^* e^{-ik(z-ct)} \mathbf{e}_-], \quad (1.30)$$

$$\mathbf{B} = \nabla \times \mathbf{A} \simeq k \sum_{n=0}^M [u_n \Psi_n e^{+ik(z-ct)} \mathbf{e}_+ + u_n^* \Psi_n^* e^{-ik(z-ct)} \mathbf{e}_-], \quad (1.31)$$

where only the time and spatial derivatives of exponent $\exp[ik(z - ct)]$ are taken into account, the radiation power P_{tot} can be written as

$$P_{tot} = \frac{\pi s_0^2}{2} c \epsilon_0 \left(ck \frac{1}{f_B} \frac{mc}{e} \right)^2 \sum_{n=0, m=0}^M u_n u_m^* e^{-i(\zeta_n - \zeta_m)} \int_0^\infty d\xi e^{-\xi} L_n(\xi) L_m(\xi). \quad (1.32)$$

Since the integral over ξ expresses the orthogonality of the GL functions, $\int_0^\infty d\xi e^{-\xi} L_n(\xi) L_m(\xi) = \delta_{nm}$, Eq. (1.32) can be written as a sum of the power P_n of each GL function

$$P_{tot}(z, z - ct) = \sum_{n=0}^M P_n \quad (1.33)$$

$$P_n(z, z - ct) = \frac{\pi s_0^2}{2} c \epsilon_0 \left(ck \frac{1}{f_B} \frac{mc}{e} \right)^2 |u_n|^2 \quad [\text{W}]. \quad (1.34)$$

Note that the z -dependence of P_n is determined by u_n only. This implies that P_n is constant outside the undulator (leaving the effect of diffraction at the mirrors out of the discussion for simplicity).

The *spectral* power, P_{tot}^s is the spectral energy density that flows with speed c through a transverse plane

$$P_{tot}^s(\kappa, z) = 2\pi \int_{r=0}^\infty r dr \frac{1}{2} (\epsilon_0 |\widetilde{\mathbf{E}}|^2 + \mu_0^{-1} |\widetilde{\mathbf{B}}|^2) c, \quad (1.35)$$

where κ denotes the frequency with respect to the frequency $\omega = ck$ of the fast phase $\exp[ik(z - ct)]$, and $\widetilde{\mathbf{E}}$ and $\widetilde{\mathbf{B}}$ are the Fourier transforms of the electric and magnetic fields Eqs. (1.30-1.31). Upon estimating these fields by

$$\widetilde{\mathbf{E}} = -\partial_t \widetilde{\mathbf{A}} \simeq ick \sum_{n=0}^M [\tilde{u}_n \Psi_n e^{+ik(z-ct)} \mathbf{e}_+ - \tilde{u}_n^* \Psi_n^* e^{-ik(z-ct)} \mathbf{e}_-], \quad (1.36)$$

$$\widetilde{\mathbf{B}} = \nabla \times \widetilde{\mathbf{A}} \simeq k \sum_{n=0}^M [\tilde{u}_n \Psi_n e^{+ik(z-ct)} \mathbf{e}_+ + \tilde{u}_n^* \Psi_n^* e^{-ik(z-ct)} \mathbf{e}_-], \quad (1.37)$$

where

$$\tilde{u}_n(z, \kappa) = \int d(z - ct) u_n(z, z - ct) e^{-i\kappa(z-ct)}, \quad (1.38)$$

is the Fourier transform of the radiation coefficient $u_n(z, z - ct)$, P_{tot}^s can be written as the sum of the spectral power of each transverse mode

$$P_{tot}^s(\kappa, z) = \sum_{n=0}^M P_n^s(\kappa, z) \quad (1.39)$$

$$P_n^s(\kappa, z) = \frac{\pi s_0^2}{2} c \epsilon_0 \left(ck \frac{1}{f_B} \frac{mc}{e} \right)^2 |\tilde{u}_n|^2 \quad [\text{Wm}^2] \quad (1.40)$$

Note that P_n^s is constant outside the undulator, just as the radiation power P_n .

1.3.3 Reflection and transmission

The reflection and transmission of radiation on the cavity mirrors plays an important role in a resonator since multiple roundtrips are required to reach saturation. In case an aperture is used, the radial mode structure changes upon reflection. This ‘scattering’ process is described by reflection and transmission matrices, which can be calculated analytically from the Huygens-Fresnel integral upon expanding both the incident and the reflected or transmitted signals into GL functions.

Reflection on the downstream mirror is considered first. Let $A_i = \sum_n u_n^i \Psi_n \exp[+ik(z-ct)]$ be the radiation propagating to the right that is incident on the mirror, and let $A_{rd} = \sum_n u_n^{rd} \Psi_n^* \exp[-ik(z+ct)]$ be the reflected radiation that propagates to the left. The radial mode structure of the incident $\{u_n^i\}$ and reflected $\{u_n^{rd}\}$ radiation is changed. This scattering process is described by

$$u_n^{rd} = -r_d \exp[2ikz - 2i\zeta_n] \sum_{m=0} \left(\frac{1-i\alpha}{1+i\alpha} \right)^{m-n} \mathcal{R}_{nm}(\xi_{ma}^d, \xi_{mr}^d) u_m^i, \quad (1.41)$$

where the minus sign arises from the boundary condition $A_{rd} + A_i = 0$ at the mirror, r_d is a real reflection coefficient that accounts for the finite conductivity of the mirrors, and α and ζ_n have to be evaluated at the position of the downstream mirror. The matrix

$$\mathcal{R}_{nm}(\xi_{ma}, \xi_{mr}) = \int_{\xi_{ma}}^{\xi_{mr}} d\xi e^{-\xi} L_n(\xi) L_m(\xi) \quad (1.42)$$

describes the changing mode structure. The quantities $\xi_{ma}^d = 2(r_{ma}^d)^2/s^2$ and $\xi_{mr}^d = 2(r_{mr}^d)^2/s^2$ are the normalized aperture and radius of the downstream mirror. The integral Eq. (1.42) is calculated analytically using the recurrence relations of the Laguerre polynomials.

The reflection on the *upstream* mirror is described by an equation similar to Eq. (1.41). Let $A_i = \sum_n u_n^i \Psi_n^* \exp[-ik(z+ct)]$ be the radiation pulse propagating to the left that is incident on the mirror, and let $A_r = \sum_n u_n^r \Psi_n \exp[+ik(z-ct)]$ be the reflected radiation pulse that propagates to the right. The scattering of the radial mode structure of the incident $\{u_n^i\}$ into the structure $\{u_n^{ru}\}$ of the reflected radiation is described by

$$u_n^{ru} = -\exp[-2ikz + 2i\zeta_n] \sum_{m=0} \left(\frac{1+i\alpha}{1-i\alpha} \right)^{m-n} \mathcal{R}_{nm}(\xi_{ma}^u, \xi_{mr}^u) u_m^i \quad (1.43)$$

where r_u is the reflection coefficient, α and ζ_n have to be evaluated at the position of the upstream mirror, and $\xi_{ma}^u = 2(r_{ma}^u)^2/s^2$ and $\xi_{mr}^u = 2(r_{mr}^u)^2/s^2$ are the normalized aperture and radius of the upstream mirror.

After being reflected by the downstream and upstream mirror, respectively, the radial mode structure $\{u_m^{out}\}$ of the pulse at the exit of the undulator is scattered into the radial structure $\{u_n^{in}\}$ at the entrance of the undulator according to

$$u_n^{in} = r_u r_d \sum_{k=0, m=0} e^{i\phi^{rt}(n,k,m)} \mathcal{R}_{nk}(\xi_{ma}^u, \xi_{mr}^u) \mathcal{R}_{km}(\xi_{ma}^d, \xi_{mr}^d) u_m^{out}, \quad (1.44)$$

where

$$\begin{aligned} \phi^{rt}(n, k, m) = 2kL_c & - 2(m + k + 1)\text{atan}\left(\frac{L_c - z_w}{l_r}\right) \\ & - 2(n + k + 1)\text{atan}\left(\frac{z_w}{l_r}\right) \end{aligned} \quad (1.45)$$

is the roundtrip phase, which is completely determined by the cavity geometry. In case of a closed resonator ($\xi_{ma} \rightarrow 0$ and $\xi_{mr} \rightarrow \infty$), Eq. (1.44) simplifies to

$$u_n^{in} = r_a r_d e^{i\phi^{rt}(n,n,n)} u_n^{out}, \quad (1.46)$$

which demonstrates that the distribution over the radiation coefficients $|u_n|^2 / |u_{n+1}|^2$ is constant. This implies that the reflection is determined by the roundtrip phase $\phi^{rt}(n, n, n)$ only.

The reflection and transmission of the radiation at the cavity mirrors requires a large number of GL functions, in particular when an aperture is present. The maximum number of GL functions that can be taken into account is limited to approximately 15 – 20, depending on the accuracy of the computer system. The limit is imposed by the algorithm used to compute the matrix elements (see Chapter 3). The main reason why one is allowed to perform numerical calculations with a finite number of GL functions is that the scattering of energy of a GL function n into other functions, which is determined by the off-diagonal ($m \neq n$) matrix elements $\mathcal{R}_{nm} \simeq \mathcal{O}(\xi_{ma}) \ll 1$, is much smaller than the energy scattered into itself. The latter is determined by the diagonal elements $\mathcal{R}_{nn} \simeq \mathcal{O}(1)$. This implies that, if the incident radiation consists of the fundamental mode $n = 0$ or of the lowest higher order modes, the reflected light will be dominated by these modes for a large number of roundtrips through the cavity, before the energy distribution $|u_n|^2$ of the higher n GL functions becomes comparable to that of the initial functions. In addition, mirror edge loss will become important for the high n GL functions, since their radial extension increases with the mode number. This leads to a strong reduction of the reflection coefficient \mathcal{R}_{nn} . The resulting energy loss is significantly larger than the fraction of energy scattered into this mode, so that the higher order GL functions will remain at a relatively low power level.

To describe the radiation amplitude that is transmitted through the hole, or along the edge of the mirror, one requires to take a large amount of GL function into account due to the fact that all matrix elements of the transmission matrix are of the same order of magnitude. This problem is overcome by computing the transmitted radiation power from radiation intensity that is incident on the mirror. For instance, the radiation power P_{ma}^d that is coupled out through the aperture in the downstream mirror is obtained from Eq. (1.29) using the appropriate boundaries

$$P_{ma}^d \propto 2\pi \int_0^{r_{ma}^d} r dr |u^i|^2 = (\pi s_0^2/2) \sum_{n=0, m=0} \left(\frac{1-i\alpha}{1+i\alpha}\right)^{n-m} \mathcal{R}_{nm}(0, \xi_{ma}^d) u_n^i u_m^{i*}, \quad (1.47)$$

where $\{u_n^i\}$ are the GL coefficients of the intra-cavity radiation, and the matrix \mathcal{R}_{nm} is given by Eq. (1.42) with ξ_{ma} and ξ_{mr} set to 0 and ξ_{ma}^d , respectively. The power that

is lost along the edges of the mirrors is also calculated from Eq. (1.47), upon replacing ξ_{ma} and ξ_{mr} to ξ_{mr}^d and ∞ , respectively.

1.3.4 Optical beam clipping by the vacuum tube

The metal vacuum tube inside the undulator will affect the radial mode structure if the diameter of the vacuum tube is comparable to or smaller than the spotsize of the radiation at the entrance or exit of the tube. In that case the radiation amplitude inside the tube must vanish at the tube edges due to a finite conductivity. This would make a decomposition of the transverse radiation profile into wave guide modes more appropriate than an expansion in GL functions. Furthermore, upon entering the tube, the radiation outside the tube edges will be cut-off.

This ‘clipping’ of the optical beam and the imposed boundary condition can be expected to have a small effect on the radial profile of the radiation if the optical mode structure is dominated by the lowest GL function ($n = 0$) and if this mode is sustained by the cavity. Under these conditions the radiation losses on the vacuum tube are estimated as mirror edges losses with effectively *smaller* radii, by following the lines of equal intensity (lines of constant $\xi = 2r^2/s^2$) of the $n = 0$ GL function from the tube edge to the cavity mirror. The effective radii are

$$r_{mr}^u|_{eff} = r_{tube} \sqrt{\frac{1 + \alpha^2(0)}{1 + \alpha^2(z_{tube1})}}, \quad r_{mr}^d|_{eff} = r_{tube} \sqrt{\frac{1 + \alpha^2(L_c)}{1 + \alpha^2(z_{tube2})}}, \quad (1.48)$$

where r_{tube} is the tube radius, and z_{tube1} and z_{tube2} is the entrance and exit of the tube with respect to the downstream mirror. This procedure leads to an increase of the transmission loss for GL functions with high ($n > 0$) mode numbers. Note that the real mirror radii are to be used if they are larger than the effective mirror radii above.

1.4 Initial conditions for the electron and radiation pulses

The electron beam in most rf-linac based FELs consists of a train of pulses. The pulse repetition rate is assumed to be such that the generated optical pulses do not interact. Under this condition, one is allowed to follow the evolution of a single radiation pulse that is repeatedly amplified by newly injected electron pulses on successive roundtrips through the cavity.

The following initial conditions for the electron and radiation pulses are considered. The electron pulse has length l_b , thus $0 \geq z - v_{pont}t \geq L_b$. The electron pulse is approximated by either a hat-shaped, a Gaussian or a parabolic longitudinal profile :

Hat-shaped profile $\mathcal{X} = 1$,

Gaussian profile $\mathcal{X} = \exp\{-[(z - v_{pont}t) - L_b/2]^2/2\sigma^2\}$, where $\sigma = L_b/6$,

Parabolic profile $\mathcal{X} = 1 - [(z - v_{pont}t) - L_b/2]^2/(L_b/2)^2$.

The transverse electron distribution is approximated by the Gaussian profile Eq. (1.10). The transverse profile is assumed to be axisymmetric upon entering the undulator, i.e. $\sigma_{x0} = \sigma_{y0}$. The pulse is divided into segments over which the density is initially constant. The segment size Δ depends on the mode of operation, as was discussed in Section 1.2.3. Within each segment, the electrons are distributed uniformly over the ponderomotive phase ψ , or nearly uniformly by including a small random phase-noise. The electrons are assumed to have a Gaussian energy distribution, proportional to

$$\exp\left[-\frac{(\delta\gamma - \langle\delta\gamma\rangle_0)^2}{2\sigma_e^2}\right], \quad (1.49)$$

where σ_e is the typical energy spread, and

$$\langle\delta\gamma\rangle_0 \equiv \frac{1}{N} \sum_{j=0}^N \delta\gamma_j = \delta\gamma_0 \mathcal{X}_{\delta\gamma}(z - v_{p0}t), \quad (1.50)$$

is the initial energy of the beam, averaged over all electrons in the segment. Here $\delta\gamma_0$ is the peak-energy detuning and the profile $\mathcal{X}_{\delta\gamma}$ allows to variate the detuning over the pulse. The electrons have with finite normalized emittance ϵ . For simplicity it is assumed that both the beam radii $\sigma_{x0} = \sigma_{y0}$, the beam emittance ϵ , and the energy spread σ_e are constant over the electron pulse. The initial *optical* pulse is assumed to have the same length as the electron pulse. Its longitudinal profile can be chosen independently (the same profiles as for the electron pulse can be selected). The initial radial mode structure is assumed to be dominated by a Gaussian mode.

The synchronization between the electron and radiation pulses at the entrance of the undulator plays an important role in the amplification process. In the absence of FEL interaction, the pulses will enter the undulator at the same instant in time if the roundtrip time $\tau_{rt} = 2L_c/c$ of the optical pulses exactly matches the repetition rate τ_{rep} . However, since the effective velocity of the radiation is reduced due to the interaction with the electrons, the optical pulse tends to enter the undulator a time L_{slip}/c later than the electron pulse. This lethargy effect leads to a reduction of the gain of the radiation, in particular when the electron pulse length is a fraction of a slippage length. The gain can be restored by shortening of the cavity by an amount ΔL , where $\Delta L = 0$ corresponds to matched pulses without FEL interaction.

Chapter 2

Numerical Implementation

The FEL model that was presented in the previous chapter is implemented in the numerical code ELIXER, which is written in FORTRAN77. The code computes the evolution of a single radiation pulse that is repeatedly amplified by a newly injected electron pulse at each roundtrip through the cavity. The amplification process is shown schematically in Fig. 2.1. The FEL experiment to be simulated is described by the input file. Optical and electron data is stored in output files at several position in the resonator. The input and output files will be discussed in Chapter 3. The discussion in this Chapter is restricted to the numerical methods used in ELIXER. Particular emphasis is put on a group of input parameters that control the stepsize and the numerical integration scheme that is used.

This Chapter is organized as follows. In Section 2.1 the normalized FEL equations that are implemented in ELIXER are derived. The numerical integration and the relevant input parameters are discussed in Section 2.2. The emphasis in Section 2.3 is on the electron and radiation grids, and on the dimensions of the data arrays involved.

2.1 ELIXER working equations

The system of FEL equations that was presented in Chapter 1 is solved by ELIXER after normalization to the so-called universal FEL scaling [13]

$$u' = u(2A_{u0}/\mu_e^2\rho^2), \quad (2.1)$$

$$p = \delta\gamma/(\gamma_r\rho/2), \quad (2.2)$$

$$z' = \rho k_u z, \quad (2.3)$$

$$(z - ct)' = \rho k(z - ct), \quad (2.4)$$

$$(z - v_{pont})' = \rho(k + k_u)(z - v_{pont}), \quad (2.5)$$

where p denotes the electron energy and the Pierce parameter

$$\rho = \left[f_B^2 \frac{4\sigma_{x0}\sigma_{y0}}{s_0^2} \left(\frac{\omega_p}{ck_u\gamma} \frac{A_u}{\sqrt{2}} \right)^2 \right]^{1/3} \ll 1 \quad (2.6)$$

is related to the beam current. This parameter is small compared to unity in any Compton-FEL. Note that the normalized undulator length is equal to $2\pi\rho N_{und}$. This

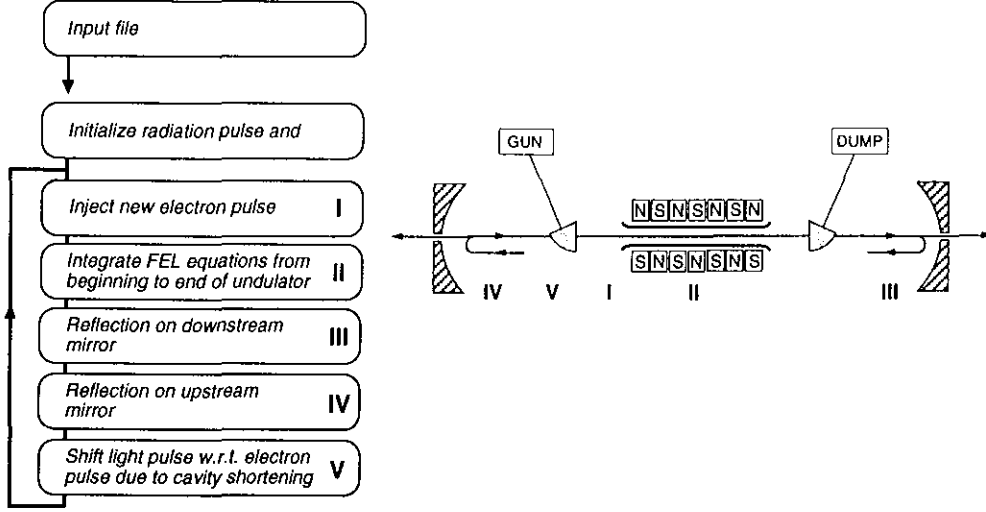


Figure 2.1: Schematic overview of the program structure. An electron pulse is bent into the optical beam line (I) and interacts with the radiation during one passage through the undulator (II). After being reflected on subsequently the downstream (II) and the upstream (IV) mirrors, the radiation pulse enters the undulator at the same instant as a newly injected electron pulse. The synchronization of the optical and electron pulses controlled by adjustment of the cavity length (V). Steps I-V are repeated to simulate the amplification over many roundtrips.

normalization transform the FEL equations to a set of ‘universal’ equations that are independent of scale lengths. Suppressing all accents for simplicity, the wave equation (1.19) becomes

$$\partial_z u_n(z, z - ct) = i I_n^* \mathcal{X} \frac{1}{N} \sum_{j=1}^N e^{-i\psi_j} = \mathcal{S}_n(z, z - v_{pont}t), \quad (2.7)$$

and the density averaged electron equations simplify to

$$\frac{d\psi_j}{dz} = p_j \quad (2.8)$$

$$\frac{dp_j}{dz} = i \sum_{n=0}^M (I_n u_n e^{i\psi_j} - I_n^* u_n^* e^{-i\psi_j}). \quad (2.9)$$

Note that the relation between the time-coordinates (1.20) simplifies to

$$z - ct = (z - v_{pont}t) - z, \quad (2.10)$$

upon using the normalization (2.1), where time coordinate $(z - v_{pont}t)$ and the undulator position z are considered to be independent variables. This system conserves the total energy of the electrons and the radiation’ i.e.

$$\partial_z \sum_{j=0}^M |u_n|^2 + \mathcal{X} \frac{1}{N} \sum_{j=1}^N \frac{d}{dz} p_j = 0. \quad (2.11)$$

2.2 Numerical control parameters and integration method

The normalized FEL equations (2.7), (2.8) and (2.9) are solved numerically using the procedure that will be discussed below. This integration process is determined by the following *numerical control parameters*

- **OPMODE** determines the mode of (electron beam) operation. Three modes of operation are distinguished as was discussed in Section 1.2.3:
OPMODE=1 Pulsed beam operation with particle tracking,
OPMODE=2 Pulsed beam operation with constant density approximation,
OPMODE=3 Continuous beam operation with constant density approximation.
- **NESCHM** determines the integration scheme for the electron equations. For a fixed pulse position, both the wave and the electron equations are ordinary differential equations of the generic form

$$dy/dz = f(y, z)$$

that can be solved using standard integration schemes [14]. One of the schemes listed below can be selected : (Δz is the stepsize)

NESCHM=1 Euler scheme

$$y(z + \Delta z) = y(z) + \Delta z \times f(y, z),$$

NESCHM=2 Second order Runge-Kutta scheme

$$\begin{aligned} k_1 &= f(y, z), \\ k_2 &= f(y + k_1, z + \Delta z), \\ y(z + \Delta z) &= y(z) + \Delta z(k_1 + k_2)/2, \end{aligned}$$

NESCHM=3 Third order Runge-Kutta scheme

$$\begin{aligned} k_1 &= f(y, z), \\ k_2 &= f(y + (1/2)k_1, z + (1/2)\Delta z), \\ k_3 &= f(y + (3/4)k_2, z + (3/4)\Delta z), \\ y(z + \Delta z) &= y(z) + \Delta z(2k_1 + 3k_2 + 4k_3)/9, \end{aligned}$$

NESCHM=4 Fourth order Runge-Kutta scheme

$$\begin{aligned} k_1 &= f(y, z), \\ k_2 &= f(y + (1/2)k_1, z + (1/2)\Delta z), \\ k_3 &= f(y + (1/2)k_2, z + (1/2)\Delta z), \\ k_4 &= f(y + k_3, z + \Delta z), \\ y(z + \Delta z) &= y(z) + \Delta z(k_1 + 2k_2 + 2k_3 + k_4)/6, \end{aligned} \tag{2.12}$$

- NUSCHM determines the integration scheme for the wave equations. Two schemes can be selected : the Euler scheme (NUSCHM=1) or the second order Runge-Kutta scheme (NUSCHM=2).
- NZSTEP determines the integration step size. The position in the undulator is discretized according to $z = \text{IZ} \Delta z$, where IZ is an integer and

$$\Delta z = 2\pi\rho/\text{NZSTEP}, \quad (2.13)$$

is the stepsize of the integration, NZSTEP being the number of z -steps per undulator period.

- FSEGM determines the segment size in the optical and electron pulses. The time-coordinates are discretized according to $z - ct = \text{IZA} \Delta$ and $z - v_{pon}t = \text{IZB} \Delta$, where the integers IZA and IZB denote the segment position in the optical and electron pulse, respectively, and

$$\Delta = 2\pi\rho \text{FSEGM}, \quad (2.14)$$

is the segment size, FSEGM being the ratio of the segmentsize and the ponderomotive wavelength. This ratio is set to unity if OPMODE>1. Upon substitution of discretized position and time coordinates in Eq. (2.10), it is straightforward to show that the segment labels IZA and IZB are related according to

$$\begin{aligned} \text{IZA} &= \text{IZB} - \text{nint}(\text{IZ} \Delta z / \Delta), & (\text{OPMODE} < 3) \\ \text{IZA} &= \text{IZB}, & (\text{OPMODE} = 3) \end{aligned} \quad (2.15)$$

where the function `nint` implies a round-off to the nearest integer. Note that the difference between time-coordinates $z - ct$ and $z - v_{pon}t$ is neglected if OPMODE=3.

The working equations (2.7), (2.8) and (2.9) are integrated according to four steps listed below.

- i At the beginning of the first roundtrip, $\text{U}(\text{N}, \text{IZA})$ is loaded with the initial radiation amplitudes $u_n(0, z - ct)$. The arrays $\text{PSI}(\text{J}, \text{IZB})$ and $\text{P}(\text{J}, \text{IZB})$ are filled with the electron phase and energy distribution, respectively, at the entrance of the undulator. The initial number of simulation electrons (N) in each segment is the same for all segments in the electron pulse. This number is taken to be much smaller than in the experiment (typically $\mathcal{O}(10^2)$ simulation-electrons are included, whereas this number is of the order of $\mathcal{O}(10^7)$ in realistic beams). Hence each simulation particle represents the dynamics of many electrons. The initial density profile $\mathcal{X}(0, z - v_{pon}t)$ is denoted by $\text{CHIN}(\text{IZB})$.

- ii Using the radiation amplitude at position IZ, the electrons coordinates $\text{PSI}(J, \text{IZB})$ and $\text{P}(J, \text{IZB})$ are ‘pushed’ to the new position $\text{IZ}+1$, using the integration scheme selected by `NESCHM`. The radiation field is evaluated at the present position¹

$$\text{JZB} \equiv \text{nint}[\text{PSI}(J, \text{IZB})/(2\pi\text{FSEGM})], \quad (2.16)$$

of each electron in the electron pulse if `OPMODE=1`, and at the electron segment position IZB under consideration if `OPMODE>1`.

- iii The radiation amplitudes $\text{U}(N, \text{IZA})$ are integrated for all IZA -positions in the pulse using the integration method selected by `NUSCHM`. The integration is performed after the complex array $\text{BF}(\text{IZB})$, which contains the average bunching factor $\mathcal{X} \frac{1}{N} \sum_{j=1}^N e^{-i\psi_j}$, has been computed from the updated electron trajectories. This array is constructed by adding the contribution of each electron to the source term at its present pulse position Eq. (2.16) if `OPMODE=1`, or, if `OPMODE>1`, at its segment position IZB :

```

Initialize BF array
Loop over initial segments and electrons per segment
  Determine pulse position JZB of electron J
    OPMODE=1 => JZB = nint( PSI(J,IZB)/(2PI FSEGM) )
    OPMODE>1 => JZB = IZB
  Add contribution of electron J to array BF at position JZB
    BF(JZB) = BF(JZB) + CHIN(IZB)/N EXP[ -i PSI(J,IZB)]

```

- iv Steps ii and iii are repeated until the end of the undulator is reached. After each integration step, the updated radiation coefficients and the electron coordinates are stored in the arrays $\text{U}(N, \text{IZA})$, $\text{PSI}(J, \text{IZB})$ and $\text{P}(J, \text{IZB})$. The reflection on the downstream and upstream mirrors and the synchronization between the pulses upon entrance of the undulator is computed subsequently.

2.3 Grids points and array dimensions

The segment label of the arrays $\text{PSI}(J, \text{IZB})$, $\text{P}(J, \text{IZB})$ and $\text{CHIN}(\text{IZB})$ lies within the interval $\text{IZB} = (0, \dots, \text{NZB})$, where NZB is the initial number of segments in the electron pulse. This number is computed from the input file. The array BF has been defined on a slightly larger interval than the electron and density arrays, i.e. $\text{IZB} = (-\text{NGEZB}, \dots, \text{NZB} + \text{NGEZB})$. This grid is enlarged by *three* ponderomotive wavelengths in case particle tracking is selected. The extension is zero in the constant density approximation (`OPMODE>1`). The relative position of the bunching factor $\text{BF}(\text{IZB})$ and the radiation field array $\text{U}(N, \text{IZA})$ is shown in Fig. 2.2 at two positions in the undulator.

¹The time-relation Eq. (2.15) is used to switch from the electron to the radiation coordinates.

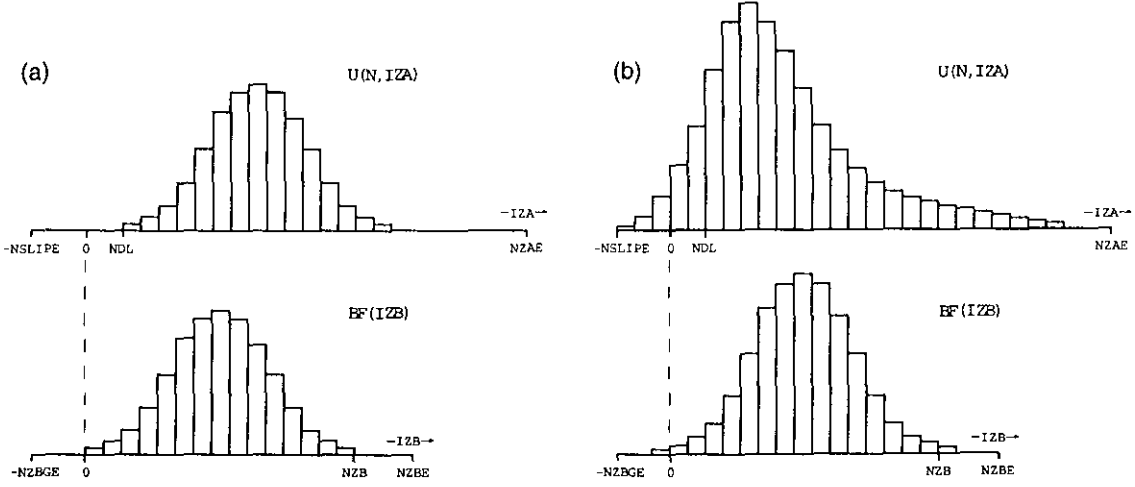


Figure 2.2: Relative position of the radiation and electron pulses at (a) the entrance and (b) the end of the undulator.

At the entrance of the undulator, the field array U is shifted to the right with respect to the bunching array BF by an amount

$$NDL = \text{nint}(2|\Delta L/\lambda_{pon}|/FSEGM)$$

due to a finite cavity shortening $\Delta L \leq 0$. After one passage through the undulator, the radiation pulse has taken over the electron pulse by $NSLIP = \text{nint}(L_{slip}/(FSEGM\lambda_{pon}))$ segments, $L_{slip} = N_{und}\lambda_{pon}$ being the slippage length. The segment label IZA in the field array U lies within the interval $IZA = (-NSLIPE, \dots, NZAE)$, where

$$NSLIPE = NSLIP + NGEZB + NGEZA|_{\Delta L > 0}, \quad (2.17)$$

$$NZAE = NZB + NGEZB + NGEZA|_{\Delta L \leq 0}, \quad (2.18)$$

The extension $NGEZA$ is used to describe the elongation of the radiation pulse due to a finite cavity shortening $\Delta L \neq 0$. The grid is extended on the leading edge side if $\Delta L \leq 0$, and on the trailing edge side if $\Delta L > 0$. The grid extension $NGEZA$ is computed as follows. When the laser reaches saturation, the radiation pulse begins to overtake over the electrons (assuming $\Delta L \leq 0$). The extension is equal to the interval set by the point where the pulses do not overlap anymore, and the point where the radiation power is reduced to $5\% = \exp(-3)$, i.e.

$$NGEZA = \text{int}(|NDL| 3/\alpha), \quad (2.19)$$

where $\alpha = (1 - r_u^2 r_d^2) + \xi_{ma}^u + \xi_{ma}^d$ accounts for absorption loss (first term) and aperture loss on the upstream and downstream mirrors, respectively (second and third term). In case perfectly conducting mirrors and zero aperture loss, the grid is extended assuming an artificial $\alpha = 5\%$ power loss per pass.

A limitation of FORTRAN is that array dimensions cannot be set dynamically. This implies that required array sizes, for instance for simulations with a large number of

segments, can exceed the pre-determined maximum values. In that case the array sizes must be enlarged in the ELIXER source code.

The arrays have the following dimensions :

<i>Name</i>	<i>Array Size</i>
PSI(J, IZB) and P(J, IZB)	J = (0, ..., NESMAX), IZB = (0, ..., NZBMAX),
CHIN(IZB)	IZB = (0, ..., NZBMAX),
SN(IZB)	IZB = (NZBGMX, ..., NZBMAX),
U(N, IZA)	N = (0, ..., MODMAX), IZA = (NSLPMAX, ..., NZAMAX).

The minimum values of the arrays SN and U must be negative (NZBGMX<0 and NSLPMAX<0).

Chapter 3

Working with ELIXER

3.1 Getting started

The ELIXER package, consisting of the source code and a number of related files, can be obtained by anonymous ftp at [zeus.rijnh.nl](ftp://zeus.rijnh.nl) in the subdirectory `revise`. The package contains the files listed below.

<i>Filename</i>	<i>Description</i>
<code>ce</code>	UNIX script for ELIXER compilation
<code>elixer.in</code>	Input file
<code>elixer.in.FEL1</code>	Input file for FELIX-FEL1
<code>elixer.in.FEL2</code>	Input file for FELIX-FEL1
<code>elixer.source</code>	REVISE source code of ELIXER
<code>manual.ps</code>	This manual
<code>radprof.source</code>	REVISE source code of radprof
<code>readme</code>	General information
<code>revise</code>	Directory containing the REVISE package

ELIXER is written with the aid of a pre-compiler from the REVISE package, which is located in the directory `revise`. The main features of the REVISE package, particularly of the pre-compiler, are discussed in Appendix A. The UNIX script file `ce` pre-compiles the ELIXER source code `elixer.source` and compiles the generated FORTRAN code consecutively into an executable file `elixer`. The input file, `elixer.in`, determines the FEL device that is to be simulated. The provided file `elixer.in` is to be used for testing purposes, since it computed only a few roundtrips through the cavity with a small amount of (simulation)-electrons and a short electron pulse. The input parameters for the two stages FEL1 and FEL2 of the Dutch FEL facility FELIX are stored in `elixer.in.FEL1-2`. Adjust these files for the FEL device of your interest. All input parameters are discussed in Section 3.2. The file `manual.ps` contains the postscript version of this document, and `radprof.source` is a utility that computes the optical energy density as a function of radial position and time from the optical mode structure $\{u_n\}$, as will be discussed in Appendix B.

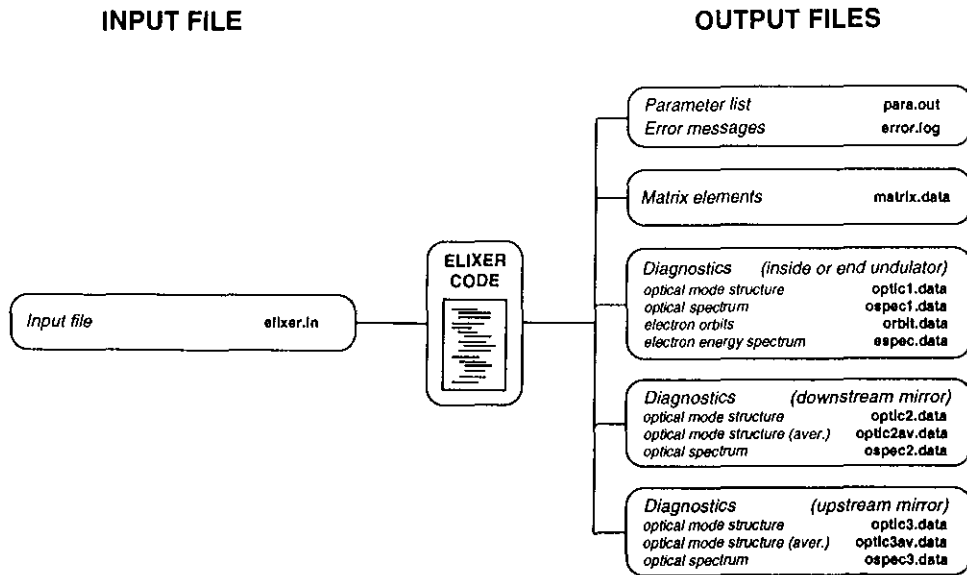


Figure 3.1: *ELIXER* input and output files.

3.2 Input file

ELIXER reads a single input file, `elixer.in`, and generates a number of output files, as is shown in Fig. 3.1. These files contain the optical mode structure of the radiation, at several positions in the resonator, and electron data as the electron energy spectrum. The output files will be discussed in Section 3.3. The emphasis in this Section is on the input file.

The input parameters are organised in six groups : (i) numerical control parameters, (ii) undulator parameters, (iii) cavity parameters, (iv) electron initial conditions, (v) radiation initial conditions and (vi) miscellaneous parameters. The parameters in each of these groups are discussed below. Only a summary of the numerical control parameters is given since they were discussed extensively in Chapter 2.

Dimensional units are used : lengths are in meters ([m]), currents in Amps ([A]), and powers in Watts ([W]).

3.2.1 Numerical control parameters

- **OPMODE** determines the mode of beam operation :
 OPMODE=1 *Pulsed beam operation with particle tracking,*
 OPMODE=2 *Pulsed beam operation with constant density approximation,*
 OPMODE=3 *Continuous beam operation with constant density approximation.*
- **NESCHM** determines the kind of integration scheme for the electron equations :
 Euler scheme (**NESCHM=1**), Runge-Kutta scheme, of second (**NESCHM=2**), third (**NESCHM=3**) and fourth order (**NESCHM=4**).
- **NUSCHM** determines the integration scheme for the wave equations : Euler scheme

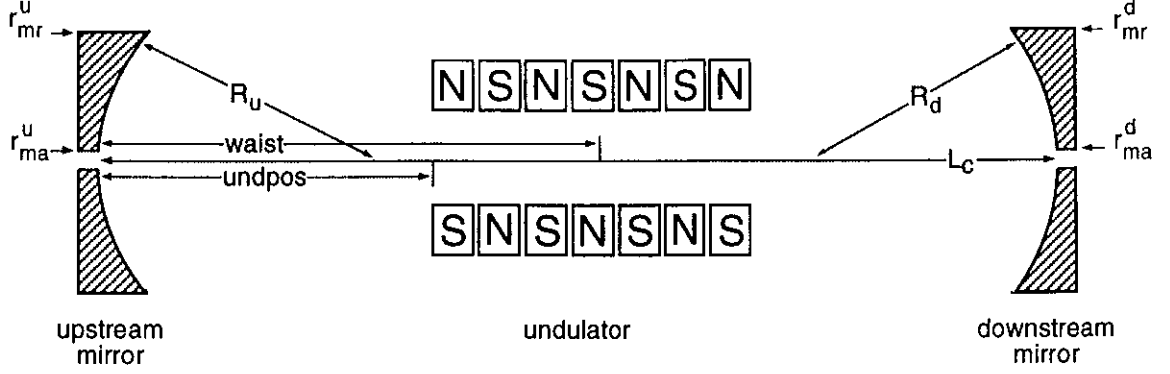


Figure 3.2: Schematic layout of the resonator.

(NUSCHM=2) and second order Runge-Kutta scheme (NUSCHM=1).

- NZSTEP is the number of z-steps per undulator period.
- FSEGM is the ratio of the segment size Δ and the ponderomotive wavelength λ_{pon} .

3.2.2 Undulator parameters

- PHFLAG determines the undulator geometry :
PHFLAG=0 implies a planar undulator,
PHFLAG=1 implies a helical undulator.
- LAMBDU is the undulator period $\lambda_u = 2\pi/k_u$.
- AU is the on-axis undulator strength A_{u0} . The rms-value has to be used in a planar undulator.
- NUND is the number of undulator periods N_{und} .
- BETFLG controls the radial inhomogeneity of the undulator magnetic field $A_u(\mathbf{x}) = A_{u0}(1 + k_x^2 x^2 + k_y^2 y^2)$:
BETFLG=0 yields a homogeneous undulator ($k_x = k_y = 0$) with a ‘cold’ electron beam (emittance is neglected),
BETFLG=1 describes an inhomogeneous undulator with a ‘warm’ beam.

3.2.3 Cavity parameters

- LCAV is the length L_c of the cavity (see Fig. 3.2).
- UNDPPOS is the position of the undulator entrance with respect to the upstream mirror.

- LRAY is the Rayleigh length l_r .
- WAIST is the position of the optical waist z_w with respect to the upstream mirror.
- CURVU is the curvature R_u of the upstream mirror.
- CURVD is the curvature R_d of the downstream mirror.
- CRVFLG determines how the Rayleigh length and waist position are computed :
 CRVFLG=0 implies that l_r and z_w are taken directly from the values of LRAY and WAIST,
 CRVFLG=1 implies that l_r and z_w are calculated from the radii of curvature of the cavity mirrors, according to Eq. (1.26).
- RU is the power reflection coefficient (r_u^2) of the upstream mirror.
- RD is the power reflection coefficient (r_d^2) of the downstream mirror.
- IDMFLG controls the transmission loss as follows :
 IDMFLG=0 implies a cavity with realistic mirrors, whose radii and apertures are listed below,
 IDMFLG=1 implies a closed resonator, in which aperture and edge loss is absent ($r_{ma} \rightarrow 0$ and $r_{mr} \rightarrow \infty$).
- APU is the aperture r_{ma} of the upstream mirror.
- RADU is the radius r_{mr} of this mirror.
- APD is the aperture r_{ma} of the downstream mirror.
- RADD is the radius r_{mr} of this mirror.
- DL is the cavity length adjustment (in units of an optical wavelength) for control of the synchronisation between the electron and radiation pulse. The difference in path length for the pulses is 2DL after one roundtrip through the cavity. The pulse are synchronized for DL=0 in the absence of a gain-medium. A negative value of DL implies a shortening of the cavity.

3.2.4 Electron initial conditions

- GAMMA0 is the relativistic factor γ_0 of the beam electrons.
 Conversion to beam energies : $\gamma_0 = 1.95 \times \text{beamenergy}$ in [MeV].
- CURR is the peak beam current I .
- SIGX0 is the 1-sigma radius $\sigma_{x0} = \sigma_{y0}$ of the Gaussian radial density profile of the electron beam.
- LB is the width L_b of the electron pulse, $0 \leq z - v_{pon}t \leq L_b$.

- MNPROF determines the longitudinal profile $\mathcal{X}(z - v_{pont})$ of the pulse. Three profiles can be selected :
MNPROF=1 Hat-shaped distribution

$$\mathcal{X}(z - v_{pont}) = 1,$$

MNPROF=2 Gaussian distribution

$$\mathcal{X}(z - v_{pont}) = \exp\{-[(z - v_{pont}) - L_b/2]^2/2\sigma^2\}, \quad \sigma = L_b/6,$$

MNPROF=3 Parabolic distribution

$$\mathcal{X}(z - v_{pont}) = 1 - [(z - v_{pont}) - L_b/2]^2/(L_b/2)^2.$$

Note that the total charge Q of the electron pulse is given by

$$Q = en2\pi\sigma_{x0}\sigma_{y0} \int d(z - v_{pont})\mathcal{X} = \frac{I}{c}L_b f_{\mathcal{X}}, \quad (3.1)$$

where $f_{\mathcal{X}} = 1, 0.42$ and 0.67 for MNPROF=1, 2 and 3, respectively.

- DETU is the peak energy detuning $\langle\delta\gamma\rangle_0/\gamma_0$.
- MANDET selects between manual or automatical calculation of the detuning :
MANDET=0 implies that the small-signal/small-gain estimate the highest single pass gain is used for the energy detuning

$$\langle\delta\gamma\rangle_0/\gamma_0 = 2.6/(4.0\pi N_u) + 1/(2k_u l_r),$$

where the second term arises from the shift of gain-detuning curve that is induced by the lowest ($n = 0$) GL function. This estimate is used for all roundtrips considered. Hence it is assumed that the lowest GL function dominates the radial mode structure of the radiation throughout the computation. MANDET=1 implies that the value of DETU is used for $\langle\delta\gamma\rangle_0/\gamma_0$.

- MPPROF determines the energy distribution $\mathcal{X}_{\delta\gamma}$ over the electron pulse. The same options as for MNPROF apply.
- SIGMAE is the 1-sigma energy spread σ_e (relative to γ_0) of the Gaussian energy distribution.
- NEMIT is the normalized emittance of the beam electrons, in units of 4π mm mrad.
- NP is the number of electrons that is used to simulate the Gaussian energy distribution in each segment of the pulse. Note that $NP \geq 1$.

- NPSI is the number of electrons that is used to simulate the ponderomotive phase distribution in each segment. Note that $NPSI \geq 1$.
- EPSPSI is the level of random phase noise (with respect to 2π) for simulation of a non-uniform phase distribution.
- MELUNI determines the *spread* in the energy-phase distributions over pulse (independent of the beam density):
MELUNI=0 implies that segment-to-segment variations are allowed,
MELUNI=1 implies that the distributions are exactly the same for each segment.

3.2.5 Radiation initial conditions

- POWER0 is the peak power level of the lowest ($n = 0$) GL function.
- MUPROF determines the longitudinal radiation power profile. The same profiles options apply as for the electron density.
- MUPHAS determines the radiation phase :
MUPHAS=0 implies that the phase is zero for all segments in the radiation pulse,
MUPHAS = 1 implies that the radiation phase in each segment is randomly distribution between $0 - 2\pi$.
- NGLMOD is the maximum number M of GL functions that is used in the simulation.
NGLMOD=0 implies that only the lowest $n = 0$ GL function is included.
- NMDPLT is the maximum number of GL functions that is used in the output files.
This number may not exceed NGLMOD.
- RELPOW is the power level of the higher order ($n > 0$) GL functions (with respect to the $n = 0$ GL function). The phases of the higher order functions are the same as that of the $n = 0$ mode.

3.2.6 Miscellaneous parameters

- NPAS is the total number of roundtrips to be computed.
- NSHDWN is the roundtrip number, after which the electron beam is switched-off.
This number may not exceed NPAS.
- PLTSTA is the roundtrip number at which the storage of the optical and electron data starts ($PLTSTA \geq 1$).
- PLTINT is the interval (in roundtrips) of this storage ($PLTINT \geq 1$).

- INTFLG determines if the optical and electron data are stored at various z -positions along the undulator (subject to the limitations set by PLTSTA and PLTINT) :
INTFLG=0 implies no intra-undulator data storage,
INTFLG=1 implies that the data is stored after each interval ZPLOT
- ZPLOT is the z -interval (in units of an undulator period) for intra-undulator data storage.
- ORBFLG controls the storage of the longitudinal electron orbits to disk: ORBFLG=1 implies that the data saved, ORBFLG=0 implies that no data is stored.
- OSFLG controls the storage of the optical spectrum. The same options as for ORBFLG apply.
- ESFLG controls the storage of the electron energy spectrum. The same options as for ORBFLG apply.
- FEXTR determines the energy interval for the electron spectra. This interval runs from $[-\delta\gamma_{max}, +\delta\gamma_{max}]$, where

$$\delta\gamma_{max} = \text{FEXTR} \frac{\gamma_r}{2N_{eff}}, \quad (3.2)$$

where $N_{eff} = N_{und}/m\mu_c$ if the slippage factor $\mu_c = N_{und}\lambda/L_b \geq 1$, and $N_{eff} = N_{und}$ otherwise.

- NRES determines the energy resolution for this spectrum ($\text{NRES} < 256$).
- ISEED is a number to start the random generator.

3.3 Output files

In this Section the contents and the structure of the output files are discussed that are generated by ELIXER (see Fig. 3.1). The file `para.out` contains relevant physical and numerical parameters that are computed from the input file, such as for instance the optical wavelength and the number of gridpoints required for the electron and optical pulses. The file `error.log` logs inconsistencies in the inputfile, such as array dimensions that exceed their maximum value. The contents and the formats of all output files (except `para.out` and `error.log`) will be discussed below.

3.3.1 Matrix elements : `matrix.data`

The file `matrix.data` contains the matrix elements of the transmission and reflection matrices \mathcal{R} . The matrix elements are stored according to the following procedure

File	matrix.data
Header	N, M, TAD, TRD, RD, TAU, TRU, RU
Data	<pre> do N=0,NGLMOD do M=0,NGLMOD write N, M, TAD(N,M), TRD(N,M), RD(N,M), TAU(N,M), TRU(N,M), RU(N,M) continue continue </pre>

where the following notation is used :

$$\text{TAD(NM)} = \mathcal{R}_{nm}(0, \xi_{ma}^d) \quad \text{TAU(NM)} = \mathcal{R}_{nm}(0, \xi_{ma}^u)$$

$$\text{TRD(NM)} = \mathcal{R}_{nm}(\xi_{mr}^d, \infty) \quad \text{TRU(NM)} = \mathcal{R}_{nm}(\xi_{ma}^u, \infty)$$

$$\text{RD(NM)} = \mathcal{R}_{nm}(\xi_{ma}^d, \xi_{mr}^d) \quad \text{RU(NM)} = \mathcal{R}_{nm}(\xi_{ma}^u, \xi_{mr}^u).$$

Here ξ_{ma}^d and ξ_{mr}^d are the normalized aperture and radius of the downstream mirror, respectively, and ξ_{ma}^u and ξ_{mr}^u are the same quantities for the upstream mirror.

The matrix elements are computed using the recurrence relations of the Laguerre polynomials as follows. Starting with the first row, or column as \mathcal{R} is symmetric (neglecting the superscripts u and d for simplicity)

$$\mathcal{R}_{00}(\xi_{ma}, \xi_{mr}) = +e^{-\xi_{ma}} - e^{-\xi_{mr}}, \quad (3.3)$$

$$\begin{aligned} \mathcal{R}_{k0}(\xi_{ma}, \xi_{mr}) = & +e^{-\xi_{ma}} [L_k(\xi_{ma}) - L_{k-1}(\xi_{ma})] \\ & - e^{-\xi_{mr}} [L_k(\xi_{mr}) - L_{k-1}(\xi_{mr})], \quad (k \geq 1) \end{aligned} \quad (3.4)$$

each reflection coefficient \mathcal{R}_{nm} with higher n and m indices can be obtained from the relation

$$\begin{aligned} \mathcal{R}_{nm}(\xi_{ma}, \xi_{mr}) = & +e^{-\xi_{ma}} L_n(\xi_{ma}) L_m(\xi_{ma}) - e^{-\xi_{mr}} L_n(\xi_{mr}) L_m(\xi_{mr}) \\ & - \sum_{i=1}^n \mathcal{R}_{n-i,m} - \sum_{j=1}^m \mathcal{R}_{n,m-j}. \end{aligned} \quad (3.5)$$

A disadvantage of this method is its sensitivity to ‘number-loss’ due of the multiple addition and subtraction of large numbers. This limits the number of GL functions that can be used in ELIXER to $\text{NGLMOD} = 15 - 20$, depending on the accuracy of the computer.

3.3.2 Optical mode structure in the undulator : optic1.data and optic1av.data

The file `optic1.data` contains the distribution of the radiation power over the transverse modes. This distribution is computed from Eq. (3.6), i.e.

$$P_{tot}(z, z - ct) = \sum_{j=0}^M P_n(z, z - ct) = \text{EFX} \sum_{j=0}^M |u_n|^2, \quad (3.6)$$

where

$$\text{EFX} = \frac{\pi s_0^2}{2} c \epsilon_0 \left(ck \frac{1}{f_B} \frac{mc \rho^2 \mu_e}{e 2A_u} \right)^2 \quad (3.7)$$

is a conversion factor to obtain the radiation power in units of Watts. The additional factor $\rho^2 \mu_e / (2A_u)$ (as compared to Eq. (3.6)) arises from the universal scaling Eq. (2.1). The power distribution is saved at the end of the undulator if `INTFLG=1`, or, if `INTFLG=0`, at equidistant positions along the undulator, where the product `ZPLOT λ_u` is the separation between the two output positions. The data stored after each interval of `PLTINT` roundtrips through the cavity, starting from roundtrip `PLTSTA`. The following data is appended to `optic1.data` for z -positions `IZ` and roundtrip numbers `IPAS` that satisfy these criteria.

File	<code>optic1.data</code>
Header	<code>PASS, Z_[M], Z-VT_[M], ABSERR_[W], RELERR, P(TOT)_[W], P(O)_[W], . . . , P(NMDPLT)_[W], PHASE(0), . . . , PHASE(NMDPLT)</code>
Data	<code>do IZA = -NSLIPE, NZAE IZB = ZAZB(IZA, IZ) write IPAS, IZ*ZTOM, IZB*ZATOM, ABSERR, RELERR, POW(-1), (POW(N), N=0, NMDPLT), (PHA(N), N=0, NMDPLT) continue,</code>

where `NMDPLT` is the maximum mode number for plotting, the arrays `POW(N)` and `PHA(N)` yield the power P_n and phase $\arg(u_n)$ of the n th GL function, respectively, and the array element `POW(-1)` contains the total power P_{tot} . The phase of each radiation coefficient is included such that the radiation amplitude within each `IZA`-segment can be reconstructed (see Appendix B). The radial pulse is evaluated in the electron coordinates (via `IZB = ZAZB(IZA, IZ)`) to facilitate a comparison of its position with respect to the electron pulse, where `ZAZB` is a function that computes the `IZA`-to-`IZB` coordinate transformation according to Eq. (2.15). The quantities

$$\text{ZTOM} = (k_u \rho)^{-1} \Delta z = \lambda_u / \text{NZSTEP}, \quad \text{and} \quad (3.8)$$

$$\text{ZATOM} = (k \rho)^{-1} \Delta = \text{FSEGM} \lambda \quad (3.9)$$

are conversion factors to obtain the position along the undulator ($z = \text{IZ} * \text{ZTOM}$) and the positions in the optical and electron pulses ($z - ct = \text{IZA} * \text{ZATOM}$ and $z - v_{pon}t \simeq \text{IZB} * \text{ZATOM}$) in units of meters. Note that the small difference between λ and λ_{pon} is neglected upon using ZATOM for the position in both pulses. Furthermore, the numerical error that is made in the integration of the radiation field and the electron trajectories is estimated from energy balance Eq. (2.11). The absolute and relative errors that are made in each integration step are given by

$$\text{ABSERR} = (\Delta u + \Delta p) \text{EFX} \quad (\text{in units of Watts}), \quad (3.10)$$

$$\text{RELERR} = (\Delta u + \Delta p) / (\Delta u - \Delta p), \quad (3.11)$$

where

$$\Delta u = \Delta z \partial_z \sum_{j=0}^M |u_n|^2 \quad \text{and} \quad \Delta p = \Delta z \mathcal{X} \frac{1}{N} \sum_{j=1}^N \frac{d}{dz} p_j$$

are the increase in radiation and electron energy as computed by ELIXER. Note that ABSERR and RELERR are zero when Eq. (2.11) is satisfied exactly.

The file `optic1av.data` contains the distribution of the radiation energy \mathcal{E} over the transverse modes. The radiation energy is the energy density, averaged over the transverse and spatial dimensions of the pulse

$$\mathcal{E} = 2\pi \int_0^\infty r dr \int d(z-ct) \frac{1}{2} (\epsilon_0 |\mathbf{E}|^2 + \mu_0^{-1} |\mathbf{B}|^2) = \int d(z-ct) P_{tot}/c. \quad (3.12)$$

Upon substitution of Eq. (3.6), \mathcal{E} can be written as a sum over the radiation energy \mathcal{E}_n of each GL function

$$\mathcal{E} = \sum_{n=0}^M \mathcal{E}_n, \quad \mathcal{E}_n = \text{PE} \sum_{\text{IZA}} |u_n|^2, \quad (3.13)$$

where $\text{PE} = (\text{EFX}/c) (\lambda \text{FSEGM})$ is a conversion factor to obtain the energy in units of Joules.

The energy distribution is stored in `optic1av.data` for each roundtrip IPAS, under the same condition on the undulator position as the data in `optic1.data`. For positions IZ that satisfy the criterium, the following data is appended to `optic1av.data`.

<i>File</i>	<code>optic1av.data</code>
<i>Header</i>	<code>PASS, Z_[M], TABSER_[J], E(TOT)_[J], E(0)_[J], . . . , E(NMDPLT)_[J]</code>
<i>Data</i>	<code>write IPAS, IZ*ZTOM, TABSER, E(-1), (E(N), N=0,NMDPLT)</code>

where the array $\text{E}(N)$ yields the energy \mathcal{E}_n of each n th GL function, $\text{E}(-1)$ contains the total pulse energy \mathcal{E}_{tot} , and the quantity TABSER is the absolute energy error ABSERR , averaged over all segments in the radiation pulse.

3.3.3 Optical mode structure at the downstream mirror : optic2.data and optic2av.data

The file `optic2.data` contains the power distribution over the transverse modes of the radiation that is reflected on the downstream mirror. This file contains also the power that is coupled out through the aperture and the power that is lost along the mirror edge. The distribution of the reflected radiation power P^{rd} over the transverse modes is given by

$$P_{tot}^{rd} = \sum_{n=0}^M P_n^{rd}, \quad P_n^{rd} = \text{EFX} |u_n^{rd}|^2, \quad (3.14)$$

where the radiation coefficients $\{u_n^{rd}\}$ are related to the coefficients $\{u_m^i\}$ of the incoming radiation according to (see Section 1.3.3)

$$u_n^{rd}(z - ct) = -r_d e^{+2ikz - 2i\zeta_n} \sum_{m=0}^M \left(\frac{1 - i\alpha}{1 + i\alpha} \right)^{m-n} \mathcal{R}_{nm}(\xi_{ma}^d, \xi_{mr}^d) u_m^i(z - ct), \quad (3.15)$$

Here z , α and ζ_n have to be evaluated at the position of the downstream mirror, \mathcal{R} is the reflection coefficient Eq. (1.42), and ξ_{ma}^d and ξ_{mr}^d are the normalized aperture and radius of the mirror. As was discussed in Section 1.3.3, in principle a large number of GL functions are required to describe the reflected radiation, due to the slow convergence (to zero) of the off-diagonal elements of the reflection matrix. However, ELIXER uses a limited number (M) of transverse modes. Therefore the reflected power P_n^{rd} (neglecting mirror absorption loss for simplicity) is slightly lower than the power P^{id} that is incident on the downstream mirror

$$P^{id}(z - ct) = \text{EFX} \sum_{n=0, m=0}^M \left(\frac{1 - i\alpha}{1 + i\alpha} \right)^{n-m} \mathcal{R}_{nm}(\xi_{ma}^d, \xi_{mr}^d) u_n^i u_m^{i*}. \quad (3.16)$$

The energy deficient is ‘repaired’ by multiplying each radiation coefficients u_n^{rd} of the reflected signal by $(P^{id}/P^{rd})^{1/2}$. This approximation assumes that the radial profile of the reflected radiation amplitude is (and remains to be) dominated by the lowest ($n < M$) GL functions. As was discussed in Section 1.3.3, this assumption is easily satisfied because of the large difference in diagonal and off-diagonal elements of the reflection matrix, and by the fact that GL functions with high mode numbers have larger edge losses than low n GL functions.

The radiation power that is lost through the aperture (P_{ma}^d) and along the mirror edge (P_{mr}^d) are not computed from a transmission matrix approach (this would require a too large number of GL functions), but from the radiation amplitude that is incident on the mirror

$$P_{ma}^d(z - ct) = \text{EFX} \sum_{n,m} \left(\frac{1 - i\alpha}{1 + i\alpha} \right)^{n-m} \mathcal{R}_{nm}(0, \xi_{ma}^d) u_n u_m^*, \quad (3.17)$$

$$P_{mr}^d(z - ct) = \text{EFX} \sum_{n,m} \left(\frac{1 - i\alpha}{1 + i\alpha} \right)^{n-m} \mathcal{R}_{nm}(\xi_{mr}^d, \infty) u_n u_m^*. \quad (3.18)$$

The reflected and transmitted signals are stored after each interval of PLTINT roundtrips through the cavity, starting from roundtrip PLTSTA. The following data is appended to optic2.data for roundtrip number IPAS that satisfy this condition.

File	optic2.data
Header	PASS, Z_[M], Z-VT_[M], PDMA_[W], PDMR_[W], PRD(TOT)_[W], PRD(0)_[W], .. , PRD(NMDPLT)_[W], PHASERD(0), .. , PHASERD(NMDPLT)
Data	do IZA = -NSLIPE,NZAE IZB = ZAZB(IZA,IZ) write IPAS, IZ*ZTOM, IZB*ZATOM, TAPOW(IZA), TRPOW(IZA), RPOW(-1), (RPOW(N), N=0,NMDPLT), (RPHA(N), N=0,NMDPLT) continue,

where the array TAPOW(N) contain the power P_{ma}^d that is lost through the aperture, and the array TRPOW(N) the power P_{mr}^d that is lost along the mirror edge. The arrays RPOW(N) and RPHA(N) denote the power P_n^{rd} and phase $\phi_n^{rd} = \arg(u_n^r)$ of the reflected radiation, respectively. The array element RPOW(-1) yields the total reflected power P_{tot}^{rd} .

The file optic2av.data contains the energy distribution over the transverse modes of the radiation that is reflected on the downstream mirror. The file also contains the energy that is lost through the aperture and along the mirror edge. The energies are computed from the reflected and transmitted radiation powers, averaged over the longitudinal dimension of the light pulse

$$\mathcal{E}^{rd} = \sum_{n=0}^M \mathcal{E}_n^{rd}, \quad \mathcal{E}_n^{rd} = \text{PE} \sum_{\text{IZA}} |u_n^{rd}|^2, \quad (3.19)$$

$$\mathcal{E}_{ma}^d = (\text{PE}/\text{EFX}) \sum_{\text{IZA}} P_{ma}^d, \quad (3.20)$$

$$\mathcal{E}_{mr}^d = (\text{PE}/\text{EFX}) \sum_{\text{IZA}} P_{mr}^d. \quad (3.21)$$

The following data is appended to optic2av.data for each roundtrip IPASS.

File	optic2av.data
Header	PASS, Z_[M], EDMA_[J], EDMR_[J], ERD(TOT)_[J], ERD(0)_[J], .. , ERD(NMDPLT)_[J]
Data	write IPAS, IZ*ZTOM, TAE, TRE, RE(-1), (RE(N), N=0,NMDPLT)

where $\text{RE}(N)$ is the reflected energy of the n th GL function \mathcal{E}_n^d , $\text{RE}(-1)$ being the total reflected energy \mathcal{E}_{tot}^d , and TAE and TRE are equal to \mathcal{E}_{ma}^d and \mathcal{E}_{mr}^d , respectively.

3.3.4 Optical mode structure at the upstream mirror : optic3.data and optic3av.data

The file `optic3.data` contains the power distribution over the transverse modes of the radiation that is reflected on the upstream mirror, as well as the power that is lost through the aperture and along the edge of this mirror. The distribution of the reflected radiation power P^{ru} over the transverse modes is given by

$$P_{tot}^{ru} = \sum_{n=0}^M P_n^{ru}, \quad P_n^{ru} = \text{EFX} |u_n^{ru}|^2, \quad (3.22)$$

where the radiation coefficients $\{u_n^{ru}\}$ are related to the coefficients $\{u_m^i\}$ of the incoming radiation according to (see Section 1.3.3)

$$u_n^{ru}(z - ct) = -r_u e^{-2ikz + 2i\zeta_n} \sum_{m=0}^M \left(\frac{1 + i\alpha}{1 - i\alpha} \right)^{m-n} \mathcal{R}_{nm}(\xi_{ma}^u, \xi_{mr}^u) u_m^i(z - ct), \quad (3.23)$$

Here z , α and ζ_n have to be evaluated at the position of the upstream mirror, \mathcal{R} is the reflection matrix Eq. (1.42), and ξ_{ma}^u and ξ_{mr}^u are the normalized aperture and mirror radius. The radiation coefficients u_n^{ru} of the reflected signal are multiplied by $(P^{iu}/P^{ru})^{1/2}$ (just as was done in Section 3.3.3) in order to account for the small decrease of the radiation power as compared to the incoming power

$$P^{iu}(z - ct) = \text{EFX} \sum_{n=0, m=0}^M \left(\frac{1 + i\alpha}{1 - i\alpha} \right)^{n-m} \mathcal{R}_{nm}(\xi_{ma}^u, \xi_{mr}^u) u_n^i u_m^{i*}. \quad (3.24)$$

The radiation power that is lost through the aperture (P_{ma}^u) and along the mirror edge (P_{mr}^u) of the upstream mirror are computed from the radiation amplitude that is incident on the mirror

$$P_{ma}^u(z - ct) = \text{EFX} \sum_{n,m} \left(\frac{1 + i\alpha}{1 - i\alpha} \right)^{n-m} \mathcal{R}_{nm}(0, \xi_{ma}^u) u_n u_m^*, \quad (3.25)$$

$$P_{mr}^u(z - ct) = \text{EFX} \sum_{n,m} \left(\frac{1 + i\alpha}{1 - i\alpha} \right)^{n-m} \mathcal{R}_{nm}(\xi_{mr}^u, \infty) u_n u_m^*. \quad (3.26)$$

The reflected and transmitted signals are stored after each interval of PLTINT roundtrips through the cavity, starting from roundtrip PLTSTA. The following data is appended to `optic3.data` for roundtrip numbers IPAS that satisfy this condition.

File	optic3.data
Header	PASS, Z_[M], Z-VT_[M], PUMA_[W], PUMR_[W], PRU(TOT)_[W], PRU(0)_[W], . . . , PRU(NMDPLT)_[W], PHASERU(0), . . . , PHASERU(NMDPLT)
Data	do IZA = -NSLIPE,NZAE IZB = ZAZB(IZA,IZ) write IPAS, IZ*ZTOM, IZB*ZATOM, TAPOW(IZA), TRPOW(IZA), RPOW(-1), (RPOW(N), N=0,NMDPLT), (RPHA(N), N=0,NMDPLT) continue,

where TAPOW(N) contains the power P_{ma}^u that is lost through the aperture, and TRPOW(N) is equal to the power P_{mr}^u that is lost along the mirror edge. The arrays RPOW(N) and RPHA(N) denote the power P_n^{ru} and phase $\arg(u_n^r)$ of the reflected radiation, respectively. The array element RPOW(-1) yields the total reflected power P_{tot}^{ru} .

The file optic3av.data contains the energy distribution over the transverse modes of the radiation that is reflected on the upstream mirror. The file also contains the energy that is lost through the aperture and along the mirror edge. The energies is computed from the reflected and transmitted radiation powers, averaged over the longitudinal dimension of the light pulse

$$\mathcal{E}^{ru} = \sum_{n=0}^M \mathcal{E}_n^{ru}, \quad \mathcal{E}_n^{ru} = \text{PE} \sum_{IZA} |u_n^{ru}|^2, \quad (3.27)$$

$$\mathcal{E}_{ma}^u = \text{PE} \sum_{IZA} (P_{ma}^u/\text{EFX}), \quad (3.28)$$

$$\mathcal{E}_{mr}^u = \text{PE} \sum_{IZA} (P_{mr}^u/\text{EFX}). \quad (3.29)$$

The following data is appended to optic3av.data for each roundtrip number IPASS.

File	optic3av.data
Header	PASS, Z_[M], EUMA_[J], EUMR_[J], ERU(TOT)_[J], ERU(0)_[J], . . . , ERU(NMDPLT)_[J]
Data	write IPAS, IZ*ZTOM, TAE, TRE, RE(-1), (RE(N), N=0,NMDPLT)

where RE(N) is the reflected energy of the n th GL function \mathcal{E}_n^{ru} , RE(-1) being the total reflected energy \mathcal{E}_{tot}^{ru} , and TAE and TRE are equal to \mathcal{E}_{ma}^u and \mathcal{E}_{mr}^u , respectively.

3.3.5 Optical power spectrum :

ospec1.data (inside the undulator),
ospec2.data (at the downstream mirror),
ospec3.data (at the upstream mirror)

The file `ospec1.data` contains the distribution of spectral power over the transverse modes. The spectral power distribution is (see Section 1.3.2)

$$P_{tot}^s(\kappa, z) = \sum_{n=0}^M P_n^s(\kappa, z) \quad (3.30)$$

$$P_n^s(\kappa, z) = \text{EFX} |\tilde{u}_n|^2 \quad [\text{Wm}^2], \quad (3.31)$$

where the conversion factor EFX is given by Eq. (3.7).

The power spectrum is computed if `OSFLG=1`. The spectral power is stored at the end of the undulator if `INTFLG=1`, or, if `INTFLG=0`, at equidistant positions along the undulator, where the product `ZPLOT λu` is the separation between the two output positions. The data stored after each interval of `PLTINT` roundtrips through the cavity, starting from roundtrip `PLTSTA`. The following data is appended to `ospec1.data` for `z`-positions `IZ` and roundtrip numbers `IPAS` that satisfy these criteria.

File	ospec1.data
Header	PASS, Z_[M], LAMBDA_[1/M], PS(TOT)_[WM2], PS(0)_[WM2], . . . , PS(NMDPLT)_[WM2]
Data	NDIM = NSLIPE+NZAE+1 do J = 1, NDIM write IPAS, IZ*ZTOM, LAMBDJ, PSTOT, (PS(N), N=0,NMDPLT) continue,

where $\text{LAMBDJ} = \lambda/[1 - (j - \text{NDIM}/2 - 1)/(\text{NDIMFSEGM})]$ is the wavelength, `PSTOT` is the total spectral power P_{tot}^s , and `PS(N)` is equal to spectral power P_n^s .

The file `ospec2.data` contains the spectral powers P_{ma}^{sd} and P_{mr}^{sd} of the radiation that is coupled out through the aperture and along the edge of the downstream mirror, respectively. The file `ospec3.data` yield the same spectral powers, but now for the upstream mirror. These spectral powers are computed from Eq. (1.32) upon using the appropriate integration boundaries, i.e.

$$P_{ma}^{sd} = \text{EFX} \sum_{n=0, m=0}^M u_n u_m^* e^{-i(\zeta_n - \zeta_m)} \mathcal{R}_{nm}(0, \xi_{ma}^d) \quad (3.32)$$

$$P_{mr}^{sd} = \text{EFX} \sum_{n=0, m=0}^M u_n u_m^* e^{-i(\zeta_n - \zeta_m)} \mathcal{R}_{nm}(0, \xi_{mr}^d) \quad (3.33)$$

and

$$P_{ma}^{su} = \text{EFX} \sum_{n=0, m=0}^M u_n u_m^* e^{+i(\zeta_n - \zeta_m)} \mathcal{R}_{nm}(0, \xi_{ma}^u) \quad (3.34)$$

$$P_{mr}^{su} = \text{EFX} \sum_{n=0, m=0}^M u_n u_m^* e^{+i(\zeta_n - \zeta_m)} \mathcal{R}_{nm}(0, \xi_{mr}^u), \quad (3.35)$$

where $\xi_{ma}^{d,u}$ and $\xi_{mr}^{d,u}$ are the normalized aperture and radius of the downstream and upstream mirrors.

This data is stored from roundtrip PLTSTA with intervals of PLTINT passes. For pass-numbers that satisfy this condition, the following data is appended to `ospec2.data` and `ospec3.data`

File	ospec2.data
Header	PASS, Z_[M], LAMBDA_[1/M], PSDMA_[WM2], PSDMR_[WM2]
Data	write IPAS, IZ*ZTOM, PSA, PSR

where PSA and PSR denote the spectral powers P_{ma}^{sd} and P_{mr}^{sd} , respectively, and

File	ospec3.data
Header	PASS, Z_[M], LAMBDA_[1/M], PSUMA_[WM2], PSUMR_[WM2]
Data	write IPAS, IZ*ZTOM, PSA, PSR

where PSA and PSR now yield the spectral powers P_{ma}^{su} and P_{mr}^{su} , respectively.

3.3.6 Electron orbits : orbit.data

The longitudinal electron trajectories of each segment in the electron pulse are saved in the file `orbit.data` if the input parameter `ORBFLG` is set to unity. The data storage is subject to the same conditions on passnumbers `IPAS` and undulator positions `IZ` as the data stored in `optic1.data`. The following data is appended to `orbit.data` for passnumber and positions that satisfy these conditions.

File	orbit.data
Header	PASS, Z_[M], Z-VT_[M], J, PSI(J), P(J)
Data	do IZB = 0, NZB do J = 1, NES write IPAS, IZ*ZTOM, IZB*ZATOM, J, PSI(J,IZB), P(J,IZB)*PTODG continue continue

where $NES = NPSI * NP$ is the initial number of electrons per segment, and $PTODG = \rho\gamma_r/2$ a conversion factor to obtain the electron energy in terms of $\delta\gamma = \gamma - \gamma_r$.

3.3.7 Electron energy spectrum : espec.data

The file `espec.data` contains the energy spectrum of the electrons, averaged over the pulse

$$f(\delta\gamma) = \int_0^{L_b} d(z - v_{pont}) \mathcal{X} \frac{1}{N} \sum_{j=1}^N \delta(\delta\gamma - \delta\gamma_j) / \int_0^{L_b} d(z - v_{pont}) \mathcal{X}. \quad (3.36)$$

Note that integral of $f(\delta\gamma)$ over the energy $\delta\gamma$ is equal to unity.

The spectrum is computed if `ESFLG=1`. The data storage is subject to the same conditions on passnumbers `IPAS` and undulator positions `IZ` as the data stored in `optic1.data`. The following data is appended to `orbit.data` for passnumber and positions that satisfy these conditions.

File	orbit.data
Header	PASS, Z_[M], PD(0), PD(1), .. , PD(NRES)
Data	write IPAS, IZ*ZTOM, (PD(L), L=0,NRES)

where the label `L` in the array `PD`, which yields the energy distribution Eq. (3.36), denotes the energy

$$\delta\gamma = -\delta\gamma_{max} + L \frac{2\delta\gamma_{max}}{NRES},$$

$\delta\gamma_{max}$ being given by Eq. (3.2) in Section 3.2.6.

Appendix A

Pre-compilation using the REVISE package

The REVISE package provides a portable facility for the systematic maintenance of large computer programs. The package was developed to control and exchange the progression of changes in numerical codes that by an international group of scientists using different computers [15]. Revise consists of the five (FORTRAN 77) programs that are listed in Table A.1.

- `pre` is a pre-compiler that converts a REVISE source file `fn.source` into a FORTRAN file `fn.f`. The latter has to be compiled into executable file using the standard FORTRAN compiler. A REVISE source file is equal to a FORTRAN file, except that common blocks are reduced to single-line instructions. The pre-compiler places the common blocks where necessary, as is shown in Table A.2.
- `new` makes a listing out `fn.list` of a source file `fn.source`. This listing contains information on absolute line numbers, line numbers per subroutine, and on the date and time. The optional parameter `l` in `new` (and also in `mod`) controls output format (see instruction in the source codes `new.f` and `mod.f`).
- `com` makes a list of modifications `mfn.modif` from an old listing `fn.list` (for instance the previous version of a code) and a new source file `nfn.source` (the

<i>UNIX script file</i>	<i>Input files</i>	<i>Output files</i>
<code>pre fn [l]</code>	<code>fn.source</code>	<code>fn.f</code>
<code>new fn [l]</code>	<code>fn.source</code>	<code>fn.list</code>
<code>com fn nfn [mfn]</code>	<code>fn.list</code> <code>nfn.source</code>	<code>mfn.modif</code>
<code>mod fn mfn [nfn] [l]</code>	<code>fn.list</code> <code>mfn.modif</code>	<code>mfn.listm</code> <code>nfn.listr</code>
<code>ext fn</code>	<code>fn.list(r)</code>	<code>fn.source</code>

Table A.1: Revise UNIX script files and their input and output files.

REVISE source file fn.source		FORTTRAN file fn.f
*COMDECK COMBLK		PROGRAM TEST
REAL A,B,C	C	
COMMON /COMBLK/ A,B,C		REAL A,B,C
*DECK MAINPROG		COMMON /COMBLK/ A,B,C
PROGRAM TEST	C	
C		Program body
*CALL COMBLK	C	
C		END
Program body		
C		
END		

Table A.2: Example of a *REVISE* source file and its pre-compiled *FORTTRAN* file.

new version of a code). If the optional filename `mfn.modif` is omitted, then a file with name `m+nfn.modif` will be created.

- `mod` creates a listing `mfn.listm` of the modification file `mfn.modif`, and creates a new listing `nfn.listr` of the modification file and the old listing `fn.list`. If the optional filename `nfn` is neglected, then the creation of this new listing is suppressed.
- `ext` converts a listing `fn.list(r)` into a source file `fn.source` (opposite of `new`).

Although these script files are written for UNIX based computers, also IBM-VM versions are available. Batch files for other computers do not exist at this moment, but it is not too complicated to write your own scripts using the UNIX scripts as examples. These script files involve the executable files `pre.o`, `new.o`, `com.o`, `mod.o` and `ext.o`. The source code of these files (`pre.f`, `new.f` etc.) is also included with the package. In the files `new.f` and `mod.f` the number of lines per page, `ILMAX`, needs to be set (depending on the local printer), and the call to `DATE` and `TIME` may need to be adjusted for the computer that is used. In `pre.f` the switches for single or block line activation need to be set.

A.1 Installation of *REVISE*

On Unix systems, *REVISE* can be installed in the following way:

- Make a directory 'revise';
- Copy `pre.f`, `new.f`, `com.f`, `mod.f`, `ext.f`, and `revise.install` in this directory;
- Edit `new.f`, `com.f`, and `pre.f` to adjust the parameters to your computer as described above;

- Compile all files by executing `revise.install` (the FORTRAN compiler `f77` in `revise.install` may need to be replaced by the name of your compiler). This creates the files `pre.o`, `new.o`, `com.o`, `mod.o`, and `ext.o`.
- Copy the script files `pre`, `new`, `com`, `mod` and `ext` to the directory 'revise', and put this directory in the search path.

Appendix B

Calculation of the radiation amplitude using RADPROF

The program RADPROF allows to compute the radiation amplitude as a function of radial position $\xi = 2r^2/s^2$ and time $z - ct$ from the optical mode structure $\{u_n\}$ that is stored in the files `optic1-3.data`. The file `radprof.source` is the REVISE source of RADPROF. This file can be (pre-)compiled using the same script file similar as `ce`, upon replacing the strings 'elixer' by 'radprof'. RADPROF reads the same input file as ELIXER.

Upon execution, the program asks for the (interactive) input below :

- The file with the optical mode structure (i.e. `optic1-3.data`);
- The roundtrip number and, if `INTFLG=1`, the z -position at which the optical mode structure has to be read from the file selected above. The optical mode structure is stored in the real arrays $\text{POW}(N, IZA) = |u_n(z - ct)|^2$ and $\text{PHA}(N, IZA) = \arg(u_n(z - ct))$.
- the position `ZEVAL` in the resonator at which the radial profile is to be evaluated,
- the maximum value, `XIMAX` of the normalized radial coordinate ξ ,
- the maximum number `NXIMAX` of radial grid points, and finally,
- the longitudinal resolution `PLOTZA`.

The following output is written in the file `prof.data`.

<pre>File prof.data</pre>
<pre>Data do IZA = -NSLIPE, NZAE, PLOTZA write (ABS(U(NXI))**2, NXI=0, NXIMAX) continue</pre>

where the total radiation amplitude $U(NXI)$ is

$$U(NXI) = \sum_{n=0}^M u_n \frac{s_0}{s} e^{-i\zeta_n} e^{-(1-i\alpha)\xi/2} L_n(\xi) \Big|_{z=\text{ZEVAL}} \quad (\text{B.1})$$

if `optic1.data` or `optic3.data` are used, and

$$U(NXI) = \sum_{n=0}^M u_n \frac{s_0}{s} e^{+i\zeta_n} e^{-(1+i\alpha)\xi/2} L_n(\xi) \Big|_{z=ZEVAL} \quad (\text{B.2})$$

in case `optic2.data` is used. Here $u_n = \text{POW}(N, IZA)^{1/2} \exp[i\text{PHA}(N, IZA)]$ is the amplitude of each radiation coefficient, and $\xi = \text{XIMAX}/NXI$.

References

- [1] W.B. Colson, Phys. Lett. **64A**, (1977) 190.
- [2] T.-M. Tran and J.S. Wurtele, Computer Physics Comm. **54** (1989) 263, J.E. La Sala, D.A.G. Deacon and T.E. Scharlemann, Nucl. Instr. and Meth. **A250** (1986) 19, S.Y. Cai, A. Bhattacharjee and T.C. Marshall, Nucl. Instr. and Meth. **A272** (1988) 481, C.M. Tang and P.A. Sprangle, IEEE J. Quantum Electron. vol. **QE-21**, no. 7 (1985) 970, P.A. Sprangle, A. Ting and C.M. Tang, Phys. Rev. Lett. **59** (1987) 202.
- [3] R.J. Bakker, C.A.J. van der Geer, D.A. Jaroszynski, A.F.M. van der Meer, D. Oepts, P.W. van Amersfoort, V. Anderegge and P.C. van Son, Nucl. Instr. and Meth. **A331** (1993) 79.
- [4] G.H.C. van Werkhoven, B. Faatz and T.J. Schep, Phys. Rev. E vol. **50**, no. 5 (1994) 4063.
- [5] G.H.C. van Werkhoven, B. Faatz and T.J. Schep, Nucl. Instr. and Meth. **A358** (1995) 304-307.
- [6] G. Dattoli, Honglie Fang, A. Torre and R. Caloi, IEEE J. Quantum Electron. **QE-28** (1992) 901.
- [7] J. Blau and W.B. Colson, Nucl. Instr. and Meth. **A318** (1992) 717.
- [8] G.H.C. van Werkhoven, B. Faatz and T.J. Schep, Nucl. Instr. and Meth. **A331** (1993) 411-415.
- [9] G.M.H. Knippels, G.H.C. van Werkhoven, E.H. haselhoff, B. Faatz, D. Oepts and P.W. van Amersfoort, Nucl. Instr. and Meth. **A358** (1995) 308-310.
- [10] G.H.C. van Werkhoven, B. Faatz and G.M.H. Knippels, Opt. Commun. **118** (1995) 551-556.
- [11] Influence of the cavity geometry on the micropulse output of FELIX in the limit-cycle regime, H.H. Weits, G.M.H. Knippels, G.H.C. van Werkhoven, D. Oepts and P.W. van Amersfoort, *to be published in the proceedings of the 17th Free-Electron Laser conference, 21-25 August 1995, Brookhaven National Laboratory, New York, USA.*

- [12] G.H.C. van Werkhoven, *Spatial structure and nonlinear dynamics of light pulses in Free-Electron Lasers*, Thesis Technische Universiteit Eindhoven (1995), ISBN 90-386-0136-0
- [13] R. Bonifacio, C. Pellegrini and L.M. Narducci, *Optics Comm.* Vol. 50 (1984) 367.
- [14] *Numerical Recipes, The Art of Scientific Computing*, W.H. Press, S.A. Teukolsky, B.P. Flannery and W.T. Vetterling, Cambridge University Press (1986).
- [15] REWISE was developed by prof.dr. J.P. Goedbloed, FOM-Instituut voor Plasmafysica 'Rijnhuizen', Postbus 1207, 3430 BE Nieuwegein.